ADVANCED FUNCTIONAL MATERIALS
www.afm-journal.de

Recent Advances and Perspectives on Powder-Based Halide Perovskite Film Processing

*Nico Leupold and Fabian Panzer**

Halide perovskites have undergone an impressive development and could be used in a wide range of optoelectronic devices, where some of them are already at the edge of commercialization, e.g., perovskite solar cells. Recently, interest in perovskites in powder form has increased, as for example, they are found to exhibit high stability and allow for easy production of large quantities. Accordingly, also the topic of processing thin and thick films on the basis of perovskite powders is currently gaining momentum. Here, perovskite powder can form the basis for both, typical wet and solvent-based processing approaches, as well as for dry processes. In this Progress Report, the recent developments of halide perovskites in powder form and of film processing approaches are summarized that are based on them. The advantages and opportunities of the different processing methods are highlighted, but their individual drawbacks and limitations are also discussed. Prospects are also pointed out and possible steps necessary to unlock the full potential of powder-based processing methods for producing high quality thick and thin perovskite layers in the future are discussed.

1. Introduction

After more than a decade of intense research, the excitement about halide perovskites, which was triggered among other things by two reports on solid-state perovskite solar cells in 2012,[1,2] seems to be unbroken. This is quite justified, since perovskite-based solar cells,[3] as well as perovskite-based LEDs,[4,5] still keep exceeding their current record efficiency levels to novel heights, and perovskite-based X-ray detectors show significantly higher sensitivities than many of their commercially established detector material counterparts.[6–8] Halide perovskite exhibit an ABX_3 structure, where A is a monovalent cation such as methylammonium (MA), formamidinium (FA), or cesium. B is a divalent cation, typically Pb^{2+} or Sn^{2+} and X is a halide anion (Cl^-, Br^-, I^-). Even though organic A-site cations are present, halide perovskites exhibit an electronic band structure, similar to classic inorganic semiconductor materials.[9] However, in contrast to inorganic semiconductors, halide perovskites are relatively soft and can be processed from solution at room temperatures or by evaporation, similar to organic semiconductors. This is also one of the reasons for the rapid development of the perovskite field. Here the most powerful processing methods for halide perovskites could be adopted from organic semiconductor research, e.g., solution-based film processing via spinning, blade coating, inkjet printing as well as by evaporation. Besides the many advantages of these processing methods such as potential for low cost, ability for upscaling, compatibility with flexible substrates, etc., however, some disadvantages were also inherited. For example, the device efficiencies of solution-processing methods that are compatible with technological upscaling such as slot die coating are still lower than the device efficiencies of the corresponding components produced by spin coating.[10,11]

While the challenge in organic semiconductor processing is to deposit the already synthesized molecules or polymers in the desired conformation in the condensed film state, the processing of halide perovskite is based on its precursor components, e.g., lead iodide (PbI_2) and methylammonium iodide (MAI), and the actual target material, i.e., the halide perovskite (e.g., $MAPbI_3$), crystallizes only during film formation. This leads to demanding processing of perovskites, where besides the film properties such as film thickness, surface roughness, and compactness, also the properties of the perovskite itself, i.e., crystallinity, grain size, stoichiometry, grain boundaries, etc. have to be considered and optimized to obtain layers that result in efficient perovskite-based optoelectronic devices.

Here a possible solution is to synthesize the perovskite first in powder form and then use the powder in a later film processing step. Powder-based processing in general is well known in the field of ceramics or metals,[12,13] and corresponding processing approaches are established in the industrial context. Also in the field of halide perovskites, the production of perovskites in powder form has been demonstrated and attracted

N. Leupold
Department of Functional Materials
University of Bayreuth
Bayreuth 95440, Germany
Dr. F. Panzer
Soft Matter Optoelectronics
University of Bayreuth
Bayreuth 95440, Germany
E-mail: fabian.panzer@uni-bayreuth.de
The ORCID identification number(s) for the author(s) of this article can be found under https://doi.org/10.1002/adfm.202007350.

DOI: 10.1002/adfm.202007350

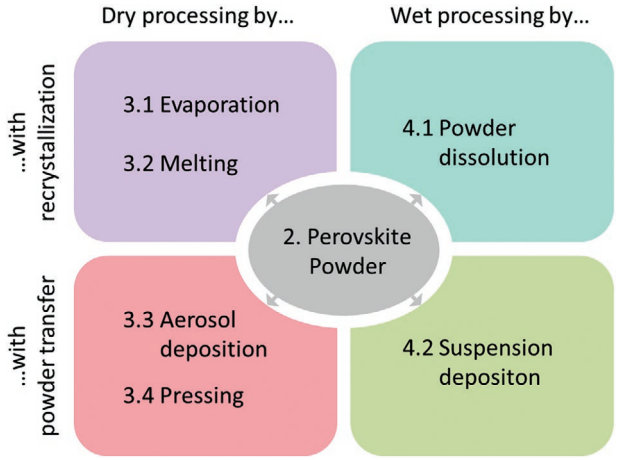

Figure 1. Schematic of the different dry (left column) and wet (right column) processing approaches that are based on perovskite powders, including methods, where the perovskite powder undergoes full dissolution and subsequent recrystallization (top row), or where the powder particles essentially remain (bottom row) in the course of the processing. The numbers refer to the corresponding sections in this Progress Report.

more and more interest in the field in the last few years.[14,15] It could be shown that, e.g., by means of mechanochemical synthesis approaches, solubility limitations of the used precursors can be circumvented, enabling the synthesis of new material compositions.[15] But also the possibility to produce large amounts of powder in a relatively short time, spurs the interest of the community in perovskite powders.[16] Also, when it comes to powder-based processing of perovskite layers, promising approaches have been shown in recent years. **Figure 1** shows an overview of the reported methods, which all have in common that readily prepared perovskite powder is used as a starting point for film or device fabrication.

The existing methods can be grouped into methods where the powder is completely dissolved during processing followed by its subsequent recrystallization (first row in Figure 1). These include physical vapor deposition, melt processing, and powder dissolution + subsequent solution processing. On the other hand, there are also approaches in which the powder essentially persists during processing and is just transferred into a layer (bottom row in Figure 1). This group includes dry powder aerosol deposition, powder pressing, and direct powder suspension deposition. Accordingly, it is also possible to distinguish between dry (left column in Figure 1) and wet (right column in Figure 1) powder-based processing methods.

In this Progress Report, we focus on the recent developments of perovskites in powder form and their film processing approaches. It structures as follows. In Section 2 we focus on the recent advancements in terms of different synthesis approaches for halide perovskites in powder form. In Section 3 we address the dry powder processing, while in Section 4 wet processing approaches are discussed. We show the current limitations of the methods but will also highlight the advantages and opportunities of powder-based halide perovskite processing, which might become a more and more important processing method in the future.

2. Halide Perovskites in Powder Form

This chapter focuses on the synthesis of halide perovskites in powder form. A short overview and comparison of the different methods (mechanochemical synthesis, thermal annealing, precipitation reactions, and ultrasonic synthesis) will be given.

2.1. Mechanochemical Synthesis

The term "mechanochemical synthesis" refers to the preparation of a target material in powder form, initiated by mechanical forces on reactants. In the simplest mechanochemical approach for halide perovskites, the individual precursor powders, e.g., MAI and PbI_2 are ground together with a mortar and pestle until the perovskite forms, typically indicated by a color change.[17] A more elaborated and controlled way to do this is by using ball mills such as shaker mills,[18] or planetary ball mills.[19] Here the reactant powders are weighed in the desired stoichiometry and poured into the milling jars together with the milling balls. The balls and milling jars are usually made of stainless steel or toughened zirconia. Sometimes a liquid grinding agent (e.g., cyclohexane) is added to carry out wet ball milling (liquid assisted grinding).[16,20] The milling jars are tightly closed, inserted into the mill and the synthesis process starts with the movement of the balls. The milling balls crush the reactants, thus providing the reaction energy by impact and friction (**Figure 2**a).

Mechanochemical synthesis has become more and more popular in recent years due to its ease of implementation and wide versatility, where the mechanochemical fabrication of halide perovskite powders was already reported by Stoumpos et al. in 2013.[21] Usually, the common binary halide salts of the type AX and BX_2 (e.g., MAI, MABr, FAI, CsI, and PbI_2, $PbBr_2$) are used as reactant powders. In the past, the mechanochemical synthesis of different halide perovskites has been demonstrated, including almost all combinations of the organic A-site cations MA^+ or FA^+ and X-site halides Cl^-, Br^- or I in the case of ternary lead halide perovskites, as well as multinary mixtures thereof.[22–25] The successful introduction of additional cations, such as guanidinium (Gua^+),[26,27] rubidium (Rb^+),[28] and especially cesium (Cs^+),[20,29,30] via mechanochemistry extends the range of available stoichiometries, including the mechanochemical synthesis of the completely inorganic halide perovskites $CsPbX_3$.[31–33] By the addition of appropriate organic molecules, it is possible to synthesize perovskite nanocrystals.[34] Furthermore, the mechanochemical synthesis of lead-free perovskites based on tin,[16,35,36] copper,[37] or bismuth[38] on the B position was demonstrated as well. Mechanochemistry is a solvent-free synthesis method. Thus, solubility limitations of precursor materials, as they are known for typical solution-based perovskite processing, do not exist. This allowed to successfully prepare mixed halide perovskites using CsCl powder as a precursor material, which cannot be dissolved in solvents that are typically used for perovskite processing.[39]

Besides the high versatility in terms of achievable compositions, mechanochemical synthesis of halide perovskites was found to exhibit further advantages. From a technological point of view, large-scale ball mills are used in many areas of industry,[12] making it easily possible to upscale the synthesis to several

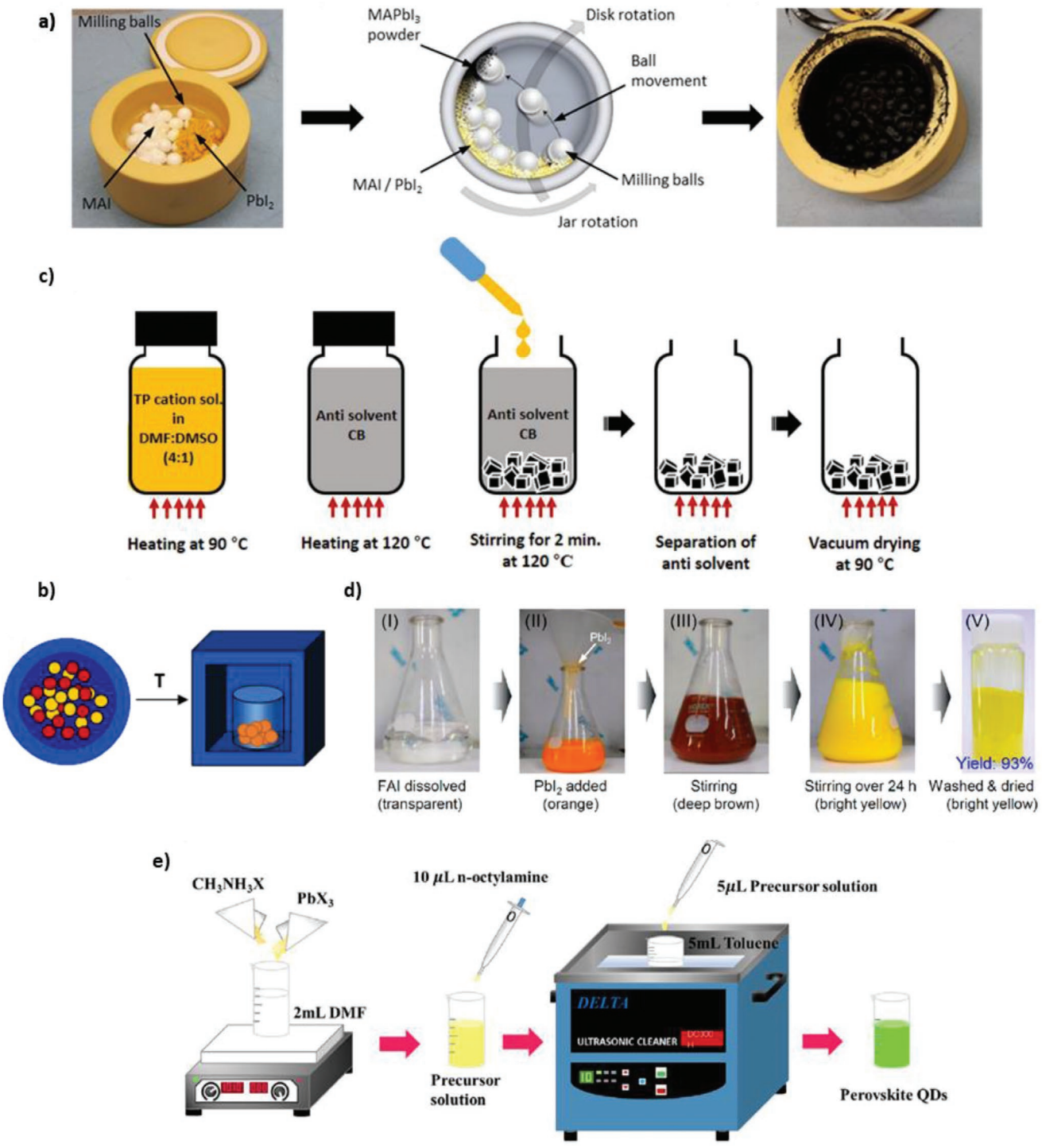

Figure 2. a) Photograph of a loaded milling jar for the mechanochemical synthesis of perovskite powder via ball milling, schematic of the ball milling procedure and photograph of the milling jar after the ball milling process and successful mechanochemical synthesis of black $MAPbI_3$ powder. b) Concept of thermal annealing synthesis of perovskite based on mixture of precursors. c) Schematic diagram for the preparation of perovskite powder via precipitation by adding precursor solution to antisolvent bath. d) Synthesis of $FAPbI_3$ powder at room temperature via a precipitation method. e) Concept of sonochemical perovskite powder synthesis using an ultrasonic bath. a) Reproduced with permission.[20] Copyright 2019, American Chemical Society. c) Reproduced with permission.[40] Copyright 2019, American Chemical Society. d) Reproduced with permission.[41] Copyright 2020, American Chemical Society. e) Reproduced with permission.[42] Copyright 2017, Elsevier B.V.

kilograms or even tons per day. This potential has also been suggested in the past for mechanochemical halide perovskite synthesis, where Tang et al. synthesized 100 g powder,[22] and Hong et al. 250 g powder in one milling jar, in one grinding cycle.[16] Here, it is interesting to note that 100 g perovskite powder transferred to layers with a thickness of 500 nm (assuming no losses) are already sufficient to cover an area of 48 m^2.

Another interesting aspect of mechanochemically synthesized perovskite powder is their high stability. $CsPbI_3$ as well as $FAPbI_3$ are promising candidates for perovskite solar cells as they exhibit potential for increased stability compared to $MAPbI_3$ and a well-suited bandgap. However, at ambient conditions, both perovskites typically degrade into an undesired non-perovskite δ-phase, where their optoelectronic properties are not suitable for preparing efficient devices anymore. Therefore, stabilizing them in their desired perovskite α-phase, where $FAPbI_3$ exhibits an even better-suited bandgap energy compared to $MAPbI_3$, is an important current research goal in the perovskite solar cell field.[43] In this context, mechanochemically synthesized $CsPbI_3$ and $FAPbI_3$ powders were found to directly crystallize in the black cubic α-phase and the degradation to the δ-phase is significantly slower than in corresponding thin films, processed via solvent-based approaches.[16,20] An overall high stability of mechanochemically synthesized perovskite powders has been repeatedly reported in literature. For example, powders can be stored for 30 d, while solutions prepared from the binary salts show signs of decomposition after only a few days.[29] When stored in dry nitrogen, $MAPbI_3$ powders do not show any decomposition signs (e.g., formation of PbI_2) even after 2.5 years, as evident from X-ray diffraction (XRD).[20] Also, perovskite powders exhibit a significantly increased thermal stability compared to their thin-film counterparts, easily withstanding exposure of 160 °C for 11 h.[20,44] Lopez et al. also observed high stability of mechanochemical $MAPbI_3$ powder regarding humidity. Compared to solvent-based powders, they attributed the increased stability to a lower inclination angle of the PbI_6 octahedrons, presumably caused by a small MA deficiency, leading to a higher Goldschmidt's tolerance factor.[45]

Another important aspect about mechanochemically synthesized perovskite powders is their ability to incorporate advances made for traditional synthesis approaches, such as solution-based synthesis approaches. In comparison to single crystals, polycrystalline perovskites exhibit a higher trap density, which increases nonradiative recombination and facilitates ion migration.[46,47] To minimize these unwanted properties, passivation strategies were developed in the past for perovskite thin film processing,[48] and transferring these passivation approaches to perovskite powders is currently gaining momentum. For example, we could show that adding K^+ to the ball milling process increases the photoluminescence (PL) of $(Cs_{0.05}FA_{0.95}PbI_3)_{0.85}(MAPbBr_3)_{0.15}$ powder, indicating successful passivation of nonradiative states. This also resulted in a reduced hysteresis of the IV-curves of solar cells that were made by spin coating of re-dissolved passivated powder.[20] The passivating effect of adamantylammonium halide compounds,[49] which has already been demonstrated for solvent-processed solar cells, could also be used to increase the PL of mechanochemically synthesized $MA_{1-y}Cs_yPb(Br_nCl_{1-n})_3$ powder, again indicating the successful passivation of non-radiative trap states.[50]

For further details about the recent progresses of the mechanochemical perovskite synthesis, we refer to the reviews of Palazon et al.,[15] Prochowicz et al.,[14] and Rosales et al.[51]

2.2. Thermal Annealing

Another solvent-free method to produce halide perovskite powders is by thermal annealing. Here, the precursor powders (AX, BX_2) are first thoroughly mixed in a chemical resistant reaction container (e.g., quartz ampoules) and sealed after mixing, to avoid evaporation of components. Heating the container for several hours to 200 to 600 °C induces the diffusion of the reactants into each other, forming the perovskite (Figure 2b). For this process, the typically high mobility of the ions in the perovskite lattice is beneficial.[51] Due to the increased temperatures, sintering processes often occur, which on the one hand increase the crystal size, but on the other hand can also have the consequence that the individual powder particles sinter together too much, so that additional milling is needed before further processing.[52] Due to the low decomposition temperature of hybrid perovskites that involve organic constituents (e.g., $MAPbI_3 \approx 240$ °C[53]), the thermal annealing approach appears to be particularly suitable for inorganic perovskites such as $CsPbX_3$, which in general exhibit an increased decomposition temperature (e.g., $CsPbBr_3 \approx 560$ °C[54]). However, mixed hybrid perovskites could be synthesized via thermal annealing when already synthesized ternary halide perovskites were used as precursors.[55]

2.3. Precipitation Reactions

Perovskite powders have also been synthesized by wet chemical methods. The approaches are similar to solvent-based thin-film processing, where the precursor salts (PbI_2, MAI, CsI, etc.) are first dissolved in suitable solvents such as dimethylformamide (DMF), acetonitrile, or γ-butyrolactone (GBL). Then, perovskite powder can be precipitated by adding an antisolvent such as ethyl acetate, chloroform, or toluene,[56,57] by pouring the precursor solution into the antisolvent (Figure 2c),[40] or by solvent evaporation.[58] For the synthesis of $FAPbI_3$ via precipitation it was found to be sufficient, to dissolve FAI in acetonitrile, add PbI_2 and stir this solution for 24 h to precipitate the perovskite (Figure 2d).[41] The shape of the resulting perovskite particles can be influenced by the solvents and by adding longer-chain organic ions. For example, adding toluene to a solution of PbI_2 and MAI in acetonitrile results in precipitation of cubic $MAPbI_3$ particles.[57] If long-chain ions such as n-octylammonium ($CH_3(CH_2)_7NH_3^+$) are added to the solution, $MAPbI_3$ nanowires precipitate. Here it was even possible to alter the aspect ratio of the nanowires by the speed at which the acetonitrile solution was added to the toluene.[57]

2.4. Sonochemical Synthesis

The ultrasonic (sonochemical) synthesis of perovskite powder is related to the solvent-based precipitation approach described

above. At first, the binary salts are dissolved or dispersed in toluene, isopropanol, DMF, or glacial acetic acid. With the help of an ultrasonic bath or a sonotrode, ultrasound is applied to the solution, inducing the crystallization of the perovskite.[59,60] The ultrasound supports dissolving reactants and also facilitates the formation of perovskite nuclei by collapsing acoustic bubbles of the precursor solution.[60] Adding organic ligands such as oleylamines to the sonochemical synthesis process also allows to produce perovskite nanocrystals (Figure 2e).[42,61] In more complex approaches, not the binary salts are used as reactants, but ion- exchange reactions are initiated by ultrasound, as shown by Jiang et al. when synthesizing $MAPbBr_3$ quantum dots from a mixture of MACl, $PbCl_2$ and KBr.[62] Furthermore, nanoplatelets of completely inorganic $CsPbX_3$ could be synthesized by using Cs_2CO_3 with PbX_2 and oleylamine and oleic acid.[63]

2.5. Outlook Halide Perovskites in Powder Form

As described above, several ways to synthesize perovskite powder exist. Similar to the classification of the different perovskite powder processing approaches from Figure 1, the synthesis approaches for perovskite powders can be divided into dry and wet methods. The wet approaches with high solvent consumption include precipitation reactions and ultrasonic synthesis, whereas the thermal annealing is completely dry. Mechanochemical synthesis is a solvent-free method, which can be performed completely dry or including small amounts of liquid to improve heat management during milling. **Table 1** gives an overview of the strengths and weaknesses of the various perovskite powder synthesis methods, which are also summarized in the following including their future prospects.

Up to now, reports on mechanochemical synthesis have mainly focused on the synthesis of a large number of stoichiometries and attempted to transfer concepts from solvent-based thin-film processing to mechanochemical synthesis. Only a few studies have focused on the impact of specific processing parameters like reactant particle sizes on the resulting perovskite, or on the reaction mechanisms.[20,64,65] Further investigations are needed to be able to adjust the powder properties more precisely. It will also be interesting to see, to which extent further passivation concepts are transferable from solvent-based processing to mechanochemically synthesized powders, and whether new passivation approaches can be realized, as the addition of passivating compounds is not limited by solubility aspects. Advantages of mechanochemistry are the high stability of the powders, and that no toxic solvents are needed. Drawbacks of the mechanochemical approach are the costs for the necessary processing equipment and that abrasion of the grinding equipment may contaminate the perovskite, thus affecting the electrical and optical properties. Furthermore, mechanochemically synthesized powders can exhibit an inhomogeneous particle size distribution, as the micrometer-sized primary particles can form dense aggregates and also tend to agglomerate (**Figure 3**a), which might have a negative impact on its further processing.

Apart from being a solvent-free synthesis approach, the attraction of thermal annealing is that it typically results in perovskite powders with large crystal size and good crystal quality. However, the necessity of relatively high temperatures limits the applicability of this synthesis approach to a limited number of halide perovskites. Furthermore, a subsequent grinding step might be necessary to crush sintered samples. Moreover, proper sealing of the reaction container (glass ampule) might become demanding on an industrial scale.

In comparison, the precipitation method requires only glass vessels and a hot plate, making it easily accessible in the lab. Additionally, it was shown that low purity reactants (<99%) are sufficient to produce powder, which after redissolving and processing to solar cells, obtains power conversion efficiencies > 21%, making the processing more cost-effective.[41] The precipitation method further scores with its ability to adjust the morphology of the powders to bulk crystals, wires, rods, and nanocrystals as can be seen in Figure 3b. But it also exhibits drawbacks as large amounts of solvent are needed and a precise adjustment of the perovskite stoichiometry can be challenging.

The advantage of ultrasonic synthesis compared to the precipitation approach is the increased dissolution rate of the reactants due to the comminuting effect of ultrasound. To the best of our knowledge, the ultrasonic synthesis of micrometer-sized perovskite powders for further processing into optoelectronic devices has not yet been reported. Thus, this route appears particularly suitable to produce nanoparticles and quantum dots (Figure 3c). However, similar to the precipitation synthesis, the sonochemical synthesis requires large amounts of solvents, which increases costs and might hamper up-scaling.

Table 1. Summary of possible strengths (top) and possible weaknesses (bottom) of different perovskite powder synthesis approaches.

Mechanochemical	Thermal annealing	Precipitation	Sonochemical
+ Up-scalable	+ Solvent-free	+ Particle morphology control possible	+ Particle morphology control possible
+ High stability	+ Large crystallite size	+ No special equipment necessary	+ Well suited for nanoparticles and quantum dots
+ Large variety	+ Well suited for inorganic halide perovskites	+ Use of low purity reactants possible	+ Facilitates educt dissolution
+ Solvent-free			
+ Possible synthesis of nanocrystals	+ Good crystal quality		
+ Precise stoichiometry control			
– Inhomogeneous particle size distribution	– Time-consuming	– Large amounts of solvents needed	– Large amounts of solvents needed
– Contamination by abrasive wear	– High temperatures needed	– Precise control of stoichiometry challenging	
– High equipment costs	– Upscaling not straight forward		
	– Difficult for hybrid perovskites		

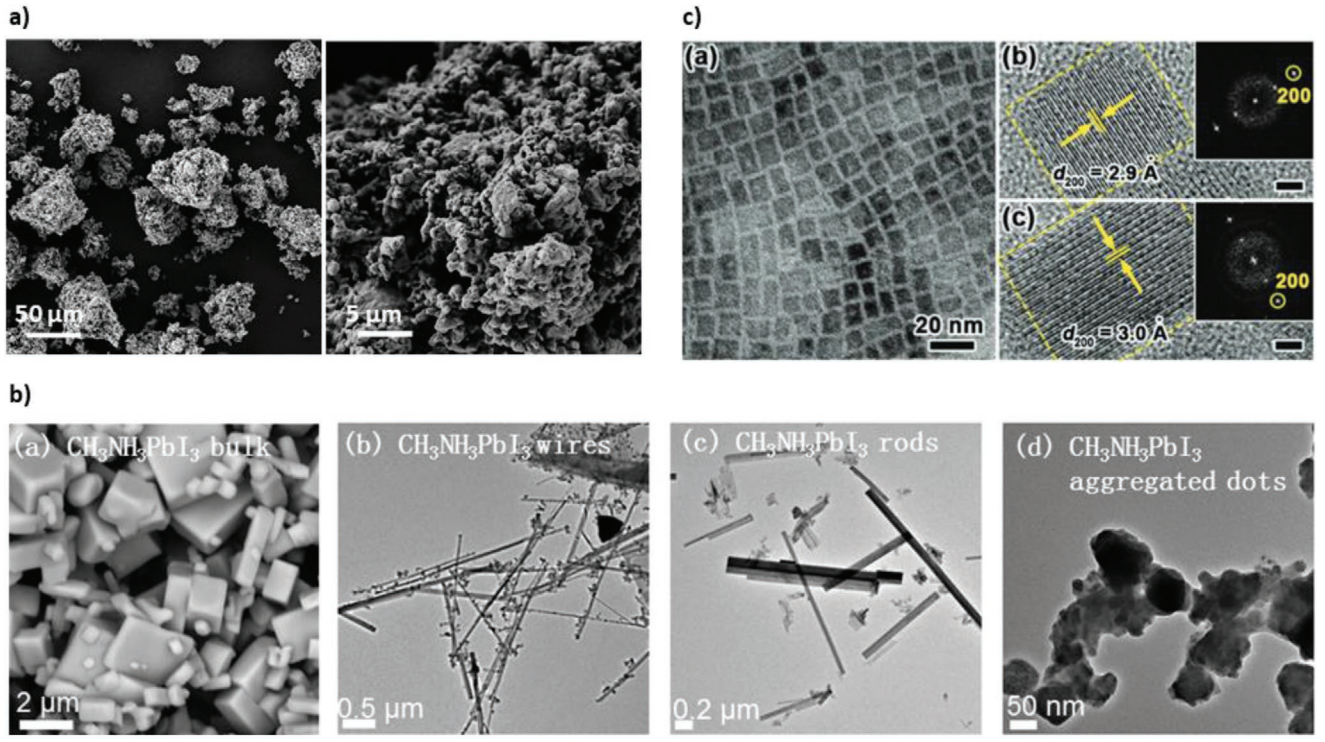

Figure 3. a) SEM image of mechanochemically synthesized $MAPbI_3$ powder via ball milling. b) Representative SEM (left) and TEM images of $MAPbI_3$ via precipitation, obtained (from left to right) without additional cations or ligands, by single fast addition, or slow addition of an acetonitrile solution containing PbI_2, CH_3NH_3I and $CH_3(CH_2)_7NH_3I$, and by single (fast) addition of a γ-butyrolactone solution containing PbI_2, CH_3NH_3I and $(H_3NCH_2CH_2CHNH_3CH_2CH_3)I_2$ to toluene. c) High-resolution TEM image of monodispersed 10 nm $CsPbBr_3$ nanocrystals synthesized via ultrasound synthesis. a) Reproduced with permission.[20] Copyright 2019, American Chemical Society. b) Reproduced with permission.[57] Copyright 2015, American Chemical Society. c) Reproduced with permission.[61] Copyright 2016, Royal Society of Chemistry.

3. Dry Powder Processing

The appeal of dry halide perovskite processing undoubtedly is connected with the potential to circumvent any safety issues due to solvent toxicity, while the potential for easy upscaling exists. Thus, e.g., the sequential or simultaneous evaporation of precursors to deposit perovskite thin films is a frequently used and well-established processing method.[66,67] Dry processing that is not based on the precursors but based on already synthesized perovskite powder is also possible and topic of this chapter. First, we will discuss methods where the perovskite structure undergoes a dissolution and subsequent recrystallizes in the course of the dry processing, which is the case for physical vapor deposition (PVD) approaches and for melt processing (3.1 and 3.2). Then we will turn to methods where the perovskite powders essentially keep their properties also during film processing, which can be achieved by powder aerosol deposition (3.3) or by powder pressing (3.4).

3.1. Physical Vapor Deposition Approaches

The preparation of compact halide perovskite films by evaporation was already demonstrated at the end of the 1990s and has become one of the most important process methods to produce halide perovskite thin films besides solution-based approaches.[67–69] In a typical evaporation process, several different precursor materials (in powder form), such as MAI and PbI_2 for the synthesis of $MAPbI_3$, are coevaporated simultaneously. The precursor powders are filled into boats or crucibles inside the vacuum chamber which is then evacuated to high vacuum. To bring the precursors into the physical vapor phase, an intense current is applied to the sources and the resulting heat leads to a thermal evaporation/sublimation of the precursor powders. As a result, perovskite film formation occurs at the substrate placed above the source powders by condensation of the material from the vapor phase. Here, the stoichiometry and deposition rate of the film can be tuned via the flux rate stemming from the different evaporation sources.

One of the most critical aspects of this method is the control of the actual deposition rates, which commonly is done via the control of the source temperatures and/or quartz crystal microbalances. The control of the deposition rate is especially challenging for the evaporation of halide perovskites involving organic cations, which tend to dissociate and have a low sticking, making the precise control of the flux rates and thus of the perovskite stoichiometry challenging.[70] A possible solution to this issue is the single-source vapor deposition (SSVD) approach, where not the individual precursors are used, but perovskite powder that is already synthesized (**Figure 4**a). In 2016, Fan et al. were the first to demonstrate the film formation of a 3D halide perovskite by this process, using already prepared $MAPbI_3$ powder, so that compact 400 nm films could be achieved, leading to efficiencies of ≈10% when used

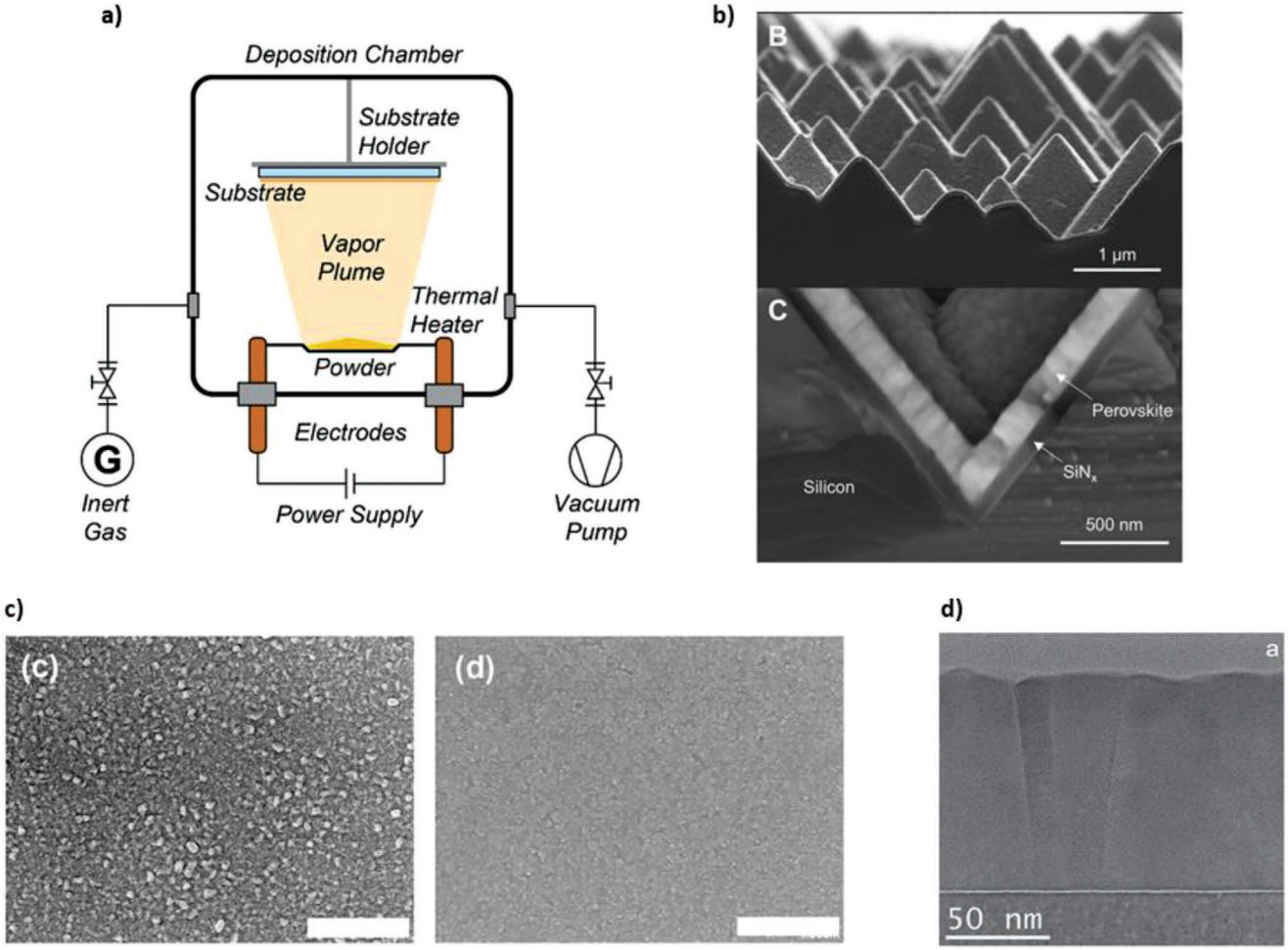

Figure 4. a) Schematic Setup for SSVD. (b) Cross-sectional SEM images of an Yb^{3+}:$CsPbCl_3$ film deposited by SSVD from a single-source powder onto a textured silicon solar cell with different magnifications. (c) Top view SEM image of SSVD processed films with thicknesses of 250 nm (left) and 890 nm (right), scale bar is 1 µm. (d) Cross-section bright-field TEM image of a γ-$CsSnI_3$ film on Si processed via pulsed laser deposition. The image shows the formation of a dense film with elongated crystalline grains. a,b) Reproduced with permission.[73] Copyright 2019, American Chemical Society. c) Reproduced with permission.[74] Copyright 2020, Wiley-VCH. d) Reproduced under the terms of the CC-BY 4.0 license.[75] Copyright 2020, the Authors. Published by Wiley-VCH.

in a solar cell.[71] Ajjouri et al. later used single source vacuum deposition to produce inorganic $CsPbX_3$ thin films, finding that compared to the individual precursors, thin films based on the perovskite powders crystallized more completely.[72] The applicability of single source vapor deposition to also complex halide perovskites such as Yb^{3+}:$CsPb(Cl_{1-x}Br_x)_3$ or highly alloyed $(FA_{0.81}MA_{0.14}Cs_{0.05})Pb(Cl_{0.02}Br_{0.14}I_{0.84})_3$ was then demonstrated by Crane et al.,[73] who also obtained very good film coverage on textured surfaces (Figure 4b). Within the past year, the perovskite powder-based SSVD film processing was also shown for other stoichiometries, with mixtures in the B-position, e.g., $CsSn_{0.3}Pb_{0.7}Br_3$ or $Cs_3Cu_2I_5$,[37,74] as well as the fabrication of layers with a relatively high thickness of 890 nm (Figure 4c). However, the latter were not phase-pure in contrast to thinner layers (250 nm), as evident from XRD measurements.[74] It was assumed that an increase in the heating times of the perovskite powder due to the higher powder quantity was responsible for the film differences. Heating up the perovskite powder sufficiently quick is a crucial aspect of SSVD, in order to minimize initial deviations in the evaporation rates of the individual constituents and to prevent material degradation, especially when organic cations are involved.[67,74]

To address this issue, Kiyek et al. recently initiated the evaporation process of perovskite powder not by applying an electric current, but by means of intense short laser pulses on a perovskite pellet (pulsed laser deposition: PLD), the latter being produced by pressing of mechanochemically synthesized perovskite source powder.[75] Using this pulsed laser deposition approach, compact $CsSnI_3$ thin films in the relevant black orthorhombic phase could be obtained, also in different thicknesses (Figure 4d). Covered by a thin Al_2O_3 layer, the PLD films exhibited a high temporal stability of several months when stored in a glovebox. Moreover, in a proof-of-principle study, Borri et al. reported the deposition of $CsPbBr_3$ using magnetron sputtering.[76] Also here, they realized the target by simple pressing of mechanochemically synthesized $CsPbBr_3$ powder. Although there is still potential in the optimization of the layer properties, i.e., in particular surface roughness

and phase purity, this work outlines an interesting alternative processing route based on perovskite powder, especially when considering the typical advantages of magnetron sputtering regarding upscaling and the possibility of easy deposition of hetero-structures.

3.2. Outlook PVD

Mainly in the past two years, the potential of perovskite powder-based physical vapor deposition approaches for the fabrication of compact, high-quality perovskite thin films of different stoichiometries has become clear. However, up to now only proof-of-concept solar cells have been built from these layers, without demonstration of highly efficient devices. Similarly, tandem solar cells such as perovskite/silicon solar cells, where the perovskite layer is processed from a powder-based PVD approach on a textured surface have, to the best of our knowledge, not yet been presented. Accordingly, it will be exciting to see how perovskite powder-based PVD approaches will develop and lead to efficient optoelectronic devices in the future. It might also be possible to realize powder-based deposition of perovskite layers with other PVD-associated methods, such as cathodic arc deposition or electron-beam physical vapor deposition.

3.3. Melt Processing

For melt processing of halide perovskites, the perovskite powder is heated above its melting temperature T_{melt} and cooled down in a systematic manner to induce and control perovskite recrystallization (**Figure 5**c). It is crucial that T_{melt} is below the material's degradation temperature to achieve complete recrystallization. The crystallization of halide perovskites from the melt was demonstrated in principle already in the early 2000s by Mitzi and co-workers, using Sn-based 2D-layered Ruddlesden-Popper perovskites.[77,78] More recently, melt film processing could also be shown for Pb-based Ruddlesden-Popper perovskites.[79] In the case of both Sn and Pb, the melting temperature was found to crucially depend on the exact properties of the organic A cation side chains.[80] Only after appropriate optimization, it was possible to reduce T_{melt} of these layered perovskites below their decomposition temperature.[77–79] The change in melt- and decomposition temperature was also suggested to be correlated with structural changes within the inorganic PbI_4 layer and/or

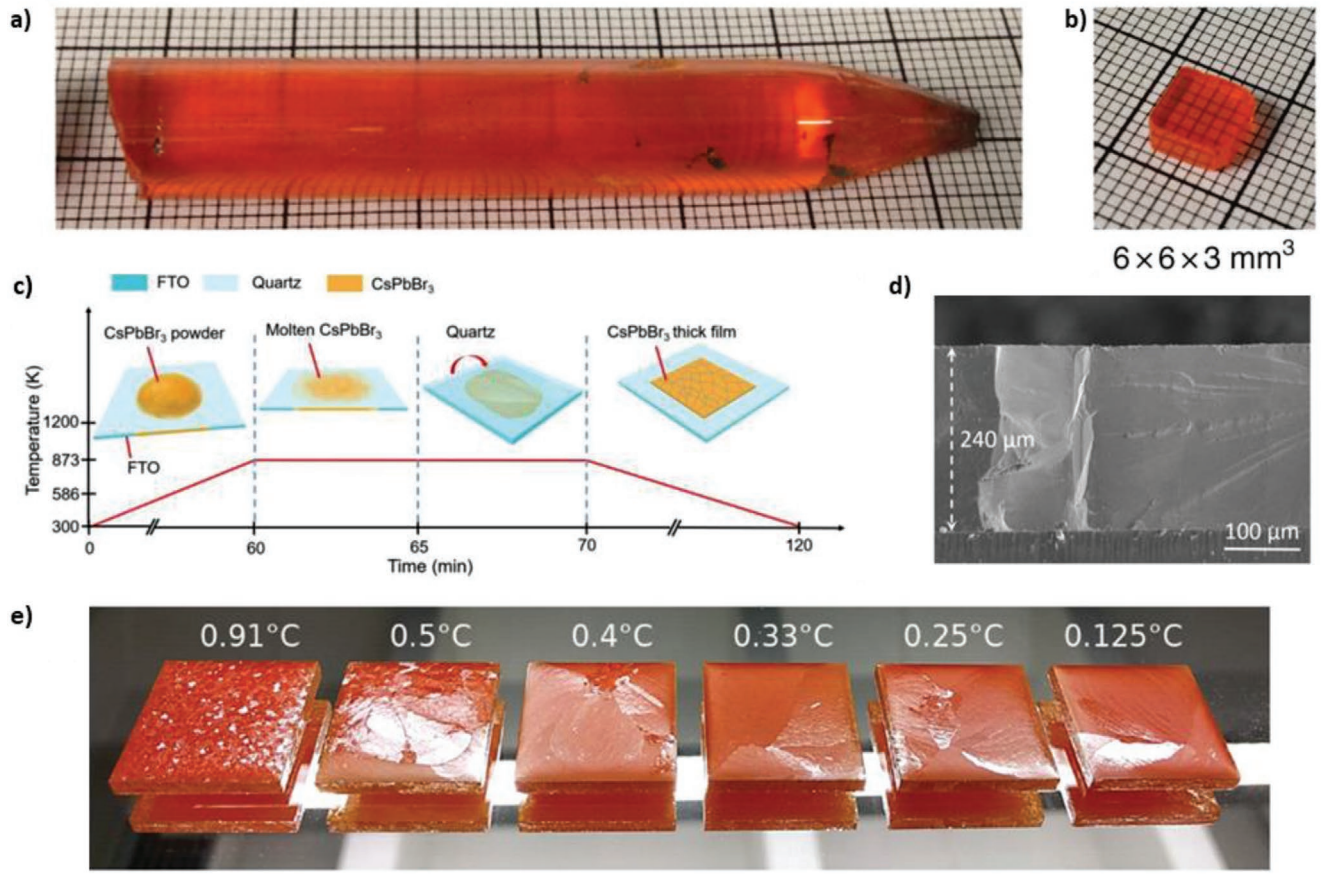

Figure 5. Photograph of a) a $CsPbBr_3$ ingot and b) a single crystal wafer grown via a Bridgman method. c) Concept of powder-based melt processing approach of $CsPbBr_3$, and d) cross-sectional SEM image of resulting thick film. e) Photographs of melt-processed $CsPbBr_3$ layers with different recrystallization rates as indicated. a,b) Reproduced under the terms of the CC-BY 4.0 license.[82] Copyright 2018, the Authors. Published by Springer Nature. c,d) Reproduced with permission.[54] Copyright 2019, Wiley-VCH. e) Reproduced under the terms of the CC BY-NC-ND 4.0 license.[83] Copyright 2020, the authors. Published by Wiley-VCH.

changes in the strength of the hydrogen bonding interaction between the inorganic and organic parts of the perovskite.[79] In a subsequent work, Mitzi and co-workers realized the melt processing of layered perovskites, in which besides longer-chain β-methylphenethylammonium (β-Me-PEA) cations, also methylammonium (MA) was introduced to a certain extent, i.e., $(\beta\text{-Me-PEA})_2MA_{n-1}Pb_nI_{3n+1}$ with $n = 1,2,3$. The introduction of MA reduced the bandgap of these perovskites, making them more relevant for optoelectronic applications such as solar cells.[81] However, it turned out that for $n > 1$, the perovskites show incongruent melting behavior upon heating and a liquid/solid mixture can develop, leading to an undesired recrystallization into different phases. Accordingly, the melt-processing needed to be followed by a further post annealing step (below the melting temperature) to cure the structural heterogeneity and successfully produce phase-pure films.[81]

In the family of 3D halide perovskites, one faces the problem that the decomposition temperature of most relevant compounds is below their melting temperature, e.g., for $MAPbI_3$ T_{decomp} = 240 °C.[53] The inorganic halide perovskite $CsPbBr_3$ is the only known exception so far, with T_{melt} of 560 °C being below the temperature range of >600 °C where degradation begins.[54] This was exploited in 2013 by Stoumpos et al. and in the following years also by other groups, so that with the help of a rather complex vertical Bridgeman method, highly crystalline $CsPbBr_3$ ingots, often of several cm in diameter and length, could be produced (Figure 5a,b).[82,84,85] Here it became clear that both, the chemical purity of the precursors,[84] and the exact cooling procedure,[82,86] are important factors influencing the optical quality (easily recognizable by the optical clarity of the ingots), as well as the electrical properties, that is the sensitivity in γ-ray or α-particle detector configuration.[82,86] Under optimized melt-recrystallization conditions, $CsPbBr_3$ ingots were found to show excellent optoelectronic properties, such as extremely low trap densities in the range of 10^9 cm^{-3},[85] and mobility-lifetime products in the range of 10^{-2} cm^2 V^{-1}.[86] Excellent optoelectronic properties of melt-processed $CsPbBr_3$ thick films used as X-ray detectors, have also been demonstrated recently by Pan et al., using a hot pressing approach.[54] Here, $CsPbBr_3$ powder was distributed onto a substrate, brought into the melt by heating to 560 °C, covered with a cover glass, and then cooled down again in a controlled manner whereby the perovskite thick film crystallized (Figure 5c).[54] Again, the use of a suitable cooling rate (in this case 5°C/min), was of decisive importance to obtain highly crystalline perovskite, even monocrystalline along the layer thickness of 240 µm (Figure 5d). Accordingly, a mobility-lifetime product of $1.3 \cdot 10^{-2}$ cm^2 V^{-1} was found, similar to corresponding values for melt-grown ingots.[86] This resulted in a record X-Ray sensitivity of 55 mC Gy_{air}^{-1} cm^{-2} at a gain factor of 3632 under an electric field of 5 V mm^{-1}.[54] Almost at the same time, Matt et al. demonstrated powder-based melt processing of 250 µm thick $CsPbBr_3$ films,[83] where in their case, the films were recrystallized with lower cooling rates in the range between 0.9 and 0.125 °C min^{-1}, and without a cover layer on the perovskite. While polycrystalline morphologies followed from fast cooling, the films obtained under low cooling rates showed large monocrystalline domains on the cm^2 scale, (Figure 5e).[83] These highly crystalline $CsPbBr_3$ thick films also showed very good X-ray sensitivities of 1450 µC Gy_{air}^{-1} cm^{-2} at 1.2×10^4 V cm^{-1} and a low lowest detectable dose rate in the range of ≈500 nGy_{air} s^{-1}.

3.4. Outlook Melt Processing

Even though halide perovskite layers with exceptional optoelectronic properties can be achieved via melt-processing, a current major drawback of this method is that its applicability is limited to perovskites that meet the precondition of $T_{melt} < T_{degradation}$. Here, the use of organic cations like MA seems to be particularly problematic. Therefore, it will be interesting to see, if other fully inorganic perovskites, perhaps even lead-free double perovskites, could be possible candidates for melt processing. In addition, the thickness of all reported melt-processed layers was in the range of hundreds of µm, so only the processing of perovskite thick films has been demonstrated yet. Accordingly, perovskite melt-processing has only been relevant for the fabrication of high energy photon detectors so far. To realize thin films by melt-processing and thus expand the pool of possible applications to, e.g., solar cells or LEDs in the future, ensuring a homogeneous powder distribution on the substrate could be an important aspect to enable compact thin layers. In this context, finding suitable strategies for a proper powder distribution, e.g., by means of powder spraying and combining it with the melt-processing might be a possible way.

In passing, we note that the characterization of perovskite layers with high crystallinity, grain size, or thickness (as they typically result by melt processing), can be more demanding compared to that of, e.g., solution-processed polycrystalline perovskite thin films. Especially in optical characterizations, measured PL spectra can significantly be influenced by self-absorption effects.[87] Thus, detailed analysis including optical modeling were applied to the measured steady-state PL spectra of thick films to extract reliable information.[88,89] Additionally, increased crystallinity and thickness can lead to increased excited state diffusion. This reduces the charge carrier density immediately after laser excitation and increases the spatial area where the excited states are present. This results in a lower photoluminescence quantum yield,[90] and thus in a decreased measured PL intensity, compared to thin films under nominally identical measurement conditions. The increased excited state diffusion also results in an accelerated PL decay typically within the first nanoseconds after laser excitation.[91] When analyzing such transient PL decays a term that considers the charge carrier diffusion needs to be added to the commonly used rate equations. This might further complicate the extraction of reliable information from time-resolved PL data of thick perovskite layers compared to their thin-film counterparts.[92]

3.5. Dry Powder Aerosol Deposition

The powder aerosol deposition (PAD) method (sometimes also referred to as aerosol deposition method, ADM) is a technology for producing dense ceramic films at room temperature directly from a ceramic powder without chemical reactions or phase transformations. It has already been used to deposit different functional materials, for example, TiO_2

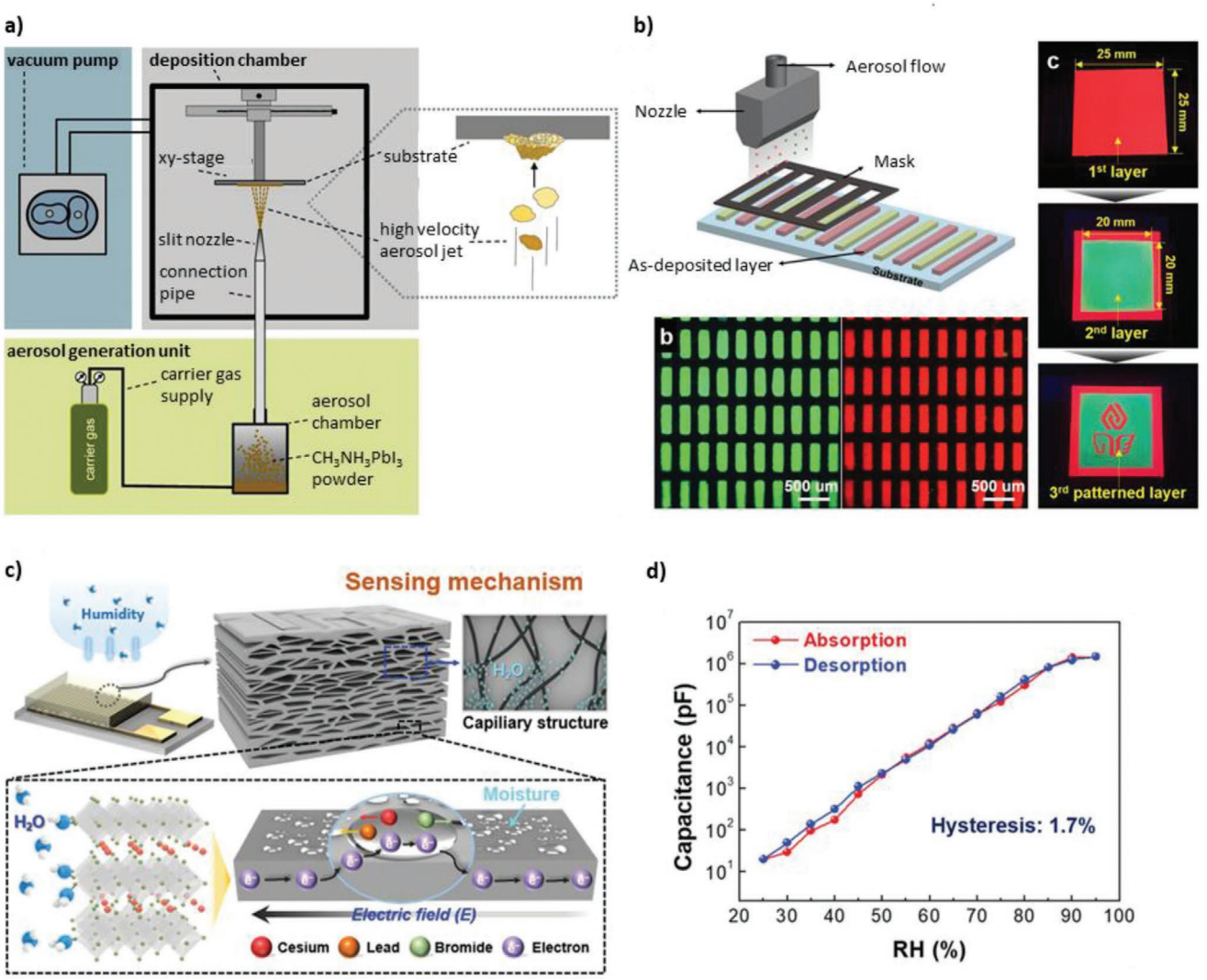

Figure 6. a) Schematic of an ADM setup. b) Schematic of patterned deposition of perovskite layers via ADM, as-deposited patterns of $CsPbBr_3$/Al_2O_3-PTFE and R-QD/Al_2O_3-PTFE nanocomposite layers. Right: R-QD/Al_2O_3-PTFE, $CsPbBr_3$/Al_2O_3-PTFE, and as-patterned R-QD/Al_2O_3-PTFE stepwise multideposition layers. c) Schematic of the humidity sensing mechanism of the $CsPb_2Br_5$/$BaTiO_3$ sensor processed via ADM. d) Hysteresis result for ADM processed $CsPb_2Br_5$/$BaTiO_3$ nanocomposite layer showing the capacitance of a function of relative humidity RH% from 25 to 95%. a) Adapted under the terms of the CC-BY 4.0 license.[105] Copyright 2016, the authors. Published by MDPI AG. b) Adapted with permission.[106] Copyright 2019, Wiley-VCH. c,d) Reproduced with permission.[107] Copyright 2020, Wiley-VCH.

for dye-sensitized solar cells,[93] $CuInGaSe_2$,[94,95] oxidic perovskites,[96,97] NiO,[98] SnO_2,[99] and CeO_2.[100] In this method, a carrier gas (e.g., N_2, He, or O_2) is lead through a powder in an aerosol chamber, forming a dry powder aerosol. The deposition chamber, in which the substrate is located, is evacuated to approximately 1 to 10 mbar by a vacuum pump. Due to the pressure difference, the dry powder aerosol transfers into the chamber via a pipe, further accelerates to 100 to 600 m s^{-1} (high velocity aerosol jet) by means of a nozzle and finally impacts on the substrate (**Figure 6**a). Upon contact with the substrate, the particles break up and form a nanocrystalline layer, which is further densified by subsequent particles due to a room temperature impact consolidation (RTIC) mechanism.[101] Details on the process can, e.g., be found in the reviews of Akedo[101] and Hanft et al.[102] For an overview on investigated materials for sensing and energy applications, we refer to the review from Schubert et al.[103] and for first commercial applications to the review by Akedo.[104]

In a proof-of-concept study, we demonstrated the fabrication of perovskite thin films using PAD in 2016.[105] Here, we obtained $MAPbI_3$ powder by simply grinding off solution-processed thin films from a glass substrate, and subsequently sprayed this powder. The perovskite layer showed good adhesion on planar TiO_2 and layer thicknesses of a few µm and even <1 µm could be realized. In particular, we could not detect any signatures of phase impurities such as PbI_2 in the measured XRD patterns of PAD-produced films and only observed typical absorption and PL properties of $MAPbI_3$, demonstrating that PAD is a non-destructive processing method for halide perovskites. However, the high surface roughness of the layers

prevented the fabrication of efficient optoelectronic devices based on the dry aerosol deposited perovskite layer.

Dry PAD was then used by Kim et al. in 2019 who sprayed $CsPbBr_3/Al_2O_3$ composite powders to produce films with a thickness in the low µm range.[106] In particular, these films showed a good long-term stability (20 d at 150 °C or > 5 months at ambient conditions) and could be processed as efficient green emitter layers in white light backlight units also including the processing of patterned shapes (Figure 6b). Furthermore, they showed the successful deposition of $CsPbBr_3/Al_2O_3$ composite on flexible substrates like polyethylene terephthalate, with high robustness against 100 000 bending cycles. In a subsequent work, the authors also use PAD to produce sensitive and particularly stable capacitive perovskite-based humidity sensors (Figure 6c).[107] For this purpose, $CsPbBr_3$ powder was deposited as a composite with other host materials such as TiO_2, Al_2O_3, and $BaTiO_3$ on gold finger electrode coated glass substrates. After suitable optimization, humidity sensors based on PAD processed $CsPb_2Br_5/BaTiO_3$ composites showed notable sensitivity with a capacitance change of 21 426 pF/RH% with a high linearity over a humidity range of 20 – 90% RH and low hysteresis (Figure 6d). Due to the use of $CsPb_2Br_5$, which is more stable than $CsPbBr_3$, and due to a suitable morphology by the surrounding $BaTiO_3$, the layers also showed a promising stability to moisture (>5 d at 90% RH).

3.6. Outlook Dry Powder Aerosol Deposition

From the three studies known to us that use dry PAD with halide perovskite powders, it already becomes clear that it is possible to transfer perovskite powders nondestructively such as to form (thin) films with good adhesion to the underlying layers. In the case of the processed composites for use as capacitive humidity sensors, a high porosity or high surface to volume ratio is desirable, which was relatively easy to achieve by PAD. For other optoelectronic applications such as lasers, LEDs or solar cells, however, the exact opposite is required, i.e., compact, dense layers with low surface roughness. To realize such PAD processed perovskite thin-film devices with decent device efficiencies in the future, optimizations regarding spraying parameters, powder properties, and especially suitable posttreatment steps to further reduce the surface roughness are necessary. In this context, suitable hot-pressing of the PAD perovskite layer could be an attractive option. Hot pressing has already been used especially in the recent past to improve both compactness and surface properties of perovskite thin films,[108–111] so that transferring hot pressing to PAD-processed films might appear achievable.

3.7. Pressing

In the past, pressing perovskite powder to pellets was often used to enable further processing methods, such as PLD or sputtering approaches.[75,76] However, the use of pellets themselves (**Figure 7**a) as active layer in optoelectronic devices was demonstrated in 2017 by Shrestha et al., who presented efficient X-ray detectors based on powder-pressed perovskite thick films.[56] For this purpose, 1 mm thick freestanding wafers were obtained by compressing $MAPbI_3$ powder with 300 MPa at room temperature. The wafers showed a density of ≈90% relative to that of a $MAPbI_3$ single crystal, and in addition, during pressing a pressure-induced sintering process occurred, which was concluded from the formation of sinter necks between perovskite particles. To transfer the freestanding wafers into a detector configuration, they were pressed onto a PEDOT:PSS coated ITO substrate at a relatively low pressure of 15 MPa for 2 min, resulting in a sufficiently high adhesion of the layer, so that a functional X-ray detector device could be produced.[56]

Similarly, Hu et al. investigated the processing of pressing perovskite powders.[115] They showed that it is possible to produce compact freestanding pellets even with a relatively low pressing pressure of 10 MPa when using elevated temperatures of 150 °C.[115] In this case, it was also possible to use only partially reacted perovskite powder that finally crystallized to phase pure $MAPbI_3$ due to the selected temperature and pressure conditions during pressing. Furthermore, they realized various wafer shapes and different layer thicknesses in the range between ≈0.1 and 1.8 mm. The resulting X-ray detector devices showed remarkable sensitivities of 1.22×10^5 µC Gy^{-1} cm^{-2} at 10 V bias voltage.

Recently, we systematically investigated the influence of pressure (Figure 7b), pressing time and temperature on the compaction dynamics occurring during the pressing of perovskite powders.[113] Using transient pressure relaxation measurements, we identified different compaction processes, namely a faster, initially dominant particle rearrangement dynamic and subsequently increasing plastic deformation dynamics of the powder particles on longer time scales (Figure 7c). Furthermore, we found that at temperatures of >≈35 °C a faster compression dynamic, presumably due to a sintering effect, occurs mainly independent of the pressure level (10–100 MPa). Under optimized pressing conditions (100 MPa, 100 °C and long-press time of ≈130 min), it was possible to produce 1 mm thick $MAPbI_3$ layers with relative densities of >97% with obvious grain growth, resulting in an average grain size of 1.9 µm.[113]

Hong et al. also used the pressing approach and pressed mechanochemically synthesized $CsSnBr_{1.5}Cl_{1.5}$ powder into 2 mm thick pellets.[16] By evaporating gold electrodes on the pellet, they realized a proof-of-concept photodetector, measuring a change of the photocurrent by about one order of magnitude under illumination using a 445 nm LED. We could also observe this qualitative proof of photocurrent, i.e., of the basic optoelectronic functionality of powder-pressed perovskite pellets, for pellets with various stoichiometries, including mixtures of A-cation and/or halides.[20] However, almost all of these powder-pressed pellets show a temporal drift or an instability of the dark current and photocurrent.[56,115,116] These current changes occur on a second to hour scale (see, e.g., drift of the baseline in Figure 7d). Besides interface effects, the migration of ions, especially of halides, is currently considered to be the main contribution to the current instabilities and also to the in general high dark currents in perovskite thick films.[117,118] Ion migration preferably occurs at the grain boundaries,[47] thus it especially limits the performance of X-ray detectors based on powder-pressed polycrystalline perovskite layers.

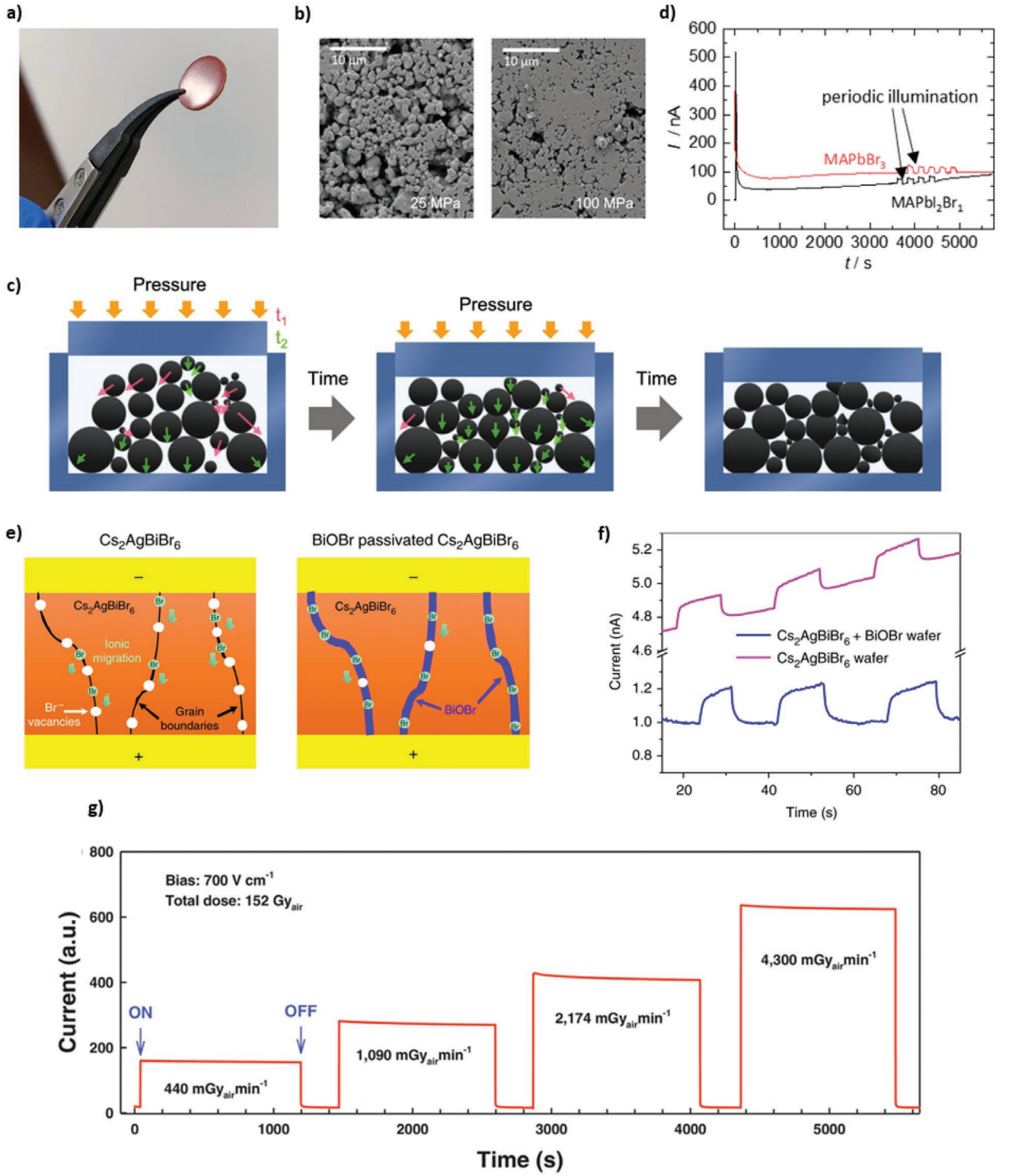

Figure 7. a) Photograph of a freestanding powder pressed $MA_3Bi_2I_9$ Pellet. b) Top-view SEM images of powder-pressed $MAPbI_3$ pellets pressed at 25 MPa (left) and 100 MPa (right). c) Illustration of the perovskite powder compaction dynamics during pressing. d) Time-resolved current of a powder pressed $MAPbBr_3$ and $MAPbI_2Br_1$ pellets at 1 V, where the samples were periodically illuminated after about 3600 s by a 405 nm laser diode. e) Schematic illustration of the suppressed ionic migration in a powder-pressed $Cs_2AgBiBr_6$ layer by BiOBr passivation. f) Performance of $Cs_2AgBiBr_6$ wafer X-ray detector with a device response to X-rays (138.7 $\mu Gy_{air}\ s^{-1}$) under an electric field of 0.1 V μm^{-1}. g) Operational stability of a powder pressed $MA_3Bi_2I_9$-powder pressed X-ray detector under 700 V cm^{-1} electric field against continuous X-ray irradiation with various dose rates from 440 to 4300 $mGy_{air}\ min^{-1}$. a,g) Reproduced with permission.[112] Copyright 2020, Wiley-VCH. b,c) Reproduced with permission.[113] Copyright 2020, American Chemical Society. d) Adapted with permission.[20] Copyright 2019, American Chemical Society. e,f) Reproduced under the terms of the CC-BY 4.0 license.[114] Copyright 2019, the authors, published by Springer Nature.

To address this issue, Yang et al. followed an epitaxial passivation strategy, where heteroepitaxial growth between BiOBr and the lead-free $CsAgBiBr_6$ perovskite derivative passivates bromide vacancies of the latter (Figure 7e).[114] They pressed, powder based on crushed $CsAgBiBr_6$ single crystals, mixed with a small proportion of BiBr to a pellet by applying 200 MPa, in an isostatic hydraulic press. Annealing this pellet at 350 °C in air for 20 h led to a significant grain size increase to about 100 µm and also initiated the epitaxial growth of BiOBr at the $CsAgBiBr_6$ grain boundaries.[114] By optical and electrical characterizations, they demonstrate the passivation of defect state at the $CsAgBiBr_6$ grain boundaries, which indeed lead to a decreased dark current, and at the same time significantly improved temporal current stability in detector configuration (Figure 7f).

Very recently, Tie et al. realized sensitive X-ray detectors by powder pressed pellets of the lead-free perovskite derivative $MA_3BI_2I_9$, which showed a sensitivity of 563 µC Gy^{-1} cm^{-2} at 2100 V cm^{-1} and low limit of detection of 9.3 nGy s^{-1}.[112] Crucial for this achievement was the high intrinsic activation energy for ion migration of 0.5 eV compared to $MAPbI_3$ with ≈0.2 eV,[119] leading to a very good temporal stability of the dark current, as well as during operation, without the need for further passivation strategies (Figure 7g). Here it is also worth noting that the high relative layer density of 97% was achieved by isostatic pressing at 200 MPa at room temperature, i.e., without further tempering. This indicates that the exact crystal structure of the perovskite is an important factor for its pressure-induced powder compaction.

As already mentioned in Section 3.3., different applications impose different requirements on the perovskite layer. For example, a high contact area of the perovskite, i.e., a high porosity of the layer, is desired for good functionality as a gas sensor material. In the case of powder pressing it is easy to achieve different degrees of compaction, as the relative density of the layer depends on the applied pressure, temperature, and pressing time.[113] Recently, Sheikh et al. took advantage of this and used a 0.6 mm thick powder pressed pellet with a relative density of 82% as an efficient ammonium sensor with low response (0.3 s) and recovery (3.6 s) times at ammonium levels as low as 10 ppm.[120]

3.8. Outlook Pressing

Powder pressing is often seen as an easily up-scalable process to produce perovskite thick films. Nevertheless, none of the pellets or layers presented so far exceed dimensions of a few cm. However, due to the low focusability of high energy optical radiation, the requirements for typical flat panel detectors are in the range of 30 × 30 cm. In the future, combinations of pressure and temperature that provide sufficiently good layer properties also on these larger scales, need to be investigated more closely. Alternatively, strategies might be required, where for example, several smaller layers might be combined to a larger one. To produce commercial powder-pressed perovskite X-ray detectors it is necessary to transfer the pressed perovskite wafers to other substrates (containing, e.g., transport layers and/or readout electronics). From our experience, achieving high adhesion between perovskite wafer and underlying substrate, while at the same time ensuring that the adhesion between perovskite and the surface of the press die is sufficiently low, can be challenging. Thus, a better understanding and control about this appears to be a desirable future goal.

4. Wet Powder Processing

In this chapter, we address wet processing approaches that are based on perovskite powders. Analogous to dry powder processing, also in the case of wet processing, it is possible to differentiate between methods where the perovskite powder is dissolved and subsequently recrystallized and wet methods, where the powder is directly transferred to a film, as will be discussed in more detail in the following.

4.1. Powder Dissolution

It might appear paradox at first sight to discard the advantages of processing dry powders by resolving them in an organic solvent (**Figure 8**a). However, it could be observed in the past that dissolving already synthesized perovskite powder and subsequent classical solution-based film processing, e.g., via spin coating, can lead to efficient perovskite solar cells.[121–127] These solar cells even showed improved performance compared to corresponding devices made from conventional reference solutions, in which the individual precursors were dissolved (Figure 8b).[18,123,124] It was found that the thin films processed from redissolved-powder-solutions exhibit bigger grains,[121–123] higher crystallinity,[121,123] lower defect density,[41,122,123] and improved stability,[41,121,123] compared to their counterparts processed from conventional precursor-based solutions (Figure 8c–f).

Prochowicz et al. attributed the improved film properties that followed from the redissolved-powder-solution processing to a purification process that takes place during the recrystallization of the perovskite.[124] This is supported by the findings of Zhang et al., who showed that even when using low-grade PbI_2 precursors, precipitated $FAPbI_3$ or $MAPbI_3$ powder exhibits a high purity due to a self-cleaning effect in the course of the precipitation process.[41,129] Dou et al. investigated the degradation of conventional precursor solutions of triple cation mixed perovskites in DMF, identifying a hydrolysis of DMF with trace water in the solution, thereby forming formic acid (HCOOH) and dimethylamine (DMA).[29] The latter impedes the subsequent crystallization of the perovskite and also leads to a faster degradation of both, thin films and solar cells that were processed from these solutions.[29] To reduce solution degradation, complex precursor solution engineering and the development of optimization strategies would be necessary. Thus, it appears attractive to circumvent this by dry storage of the perovskite in powder form and dissolve it directly prior to solution processing. But even redissolved-powder-solutions were found to show better stability compared to conventional precursor-based solutions. This was recently investigated by Shin et al. for $FAPbI_3$ precursor solutions, where either FAI and PbI_2 or presynthesized $FAPbI_3$ powder were solved in a dimethyl

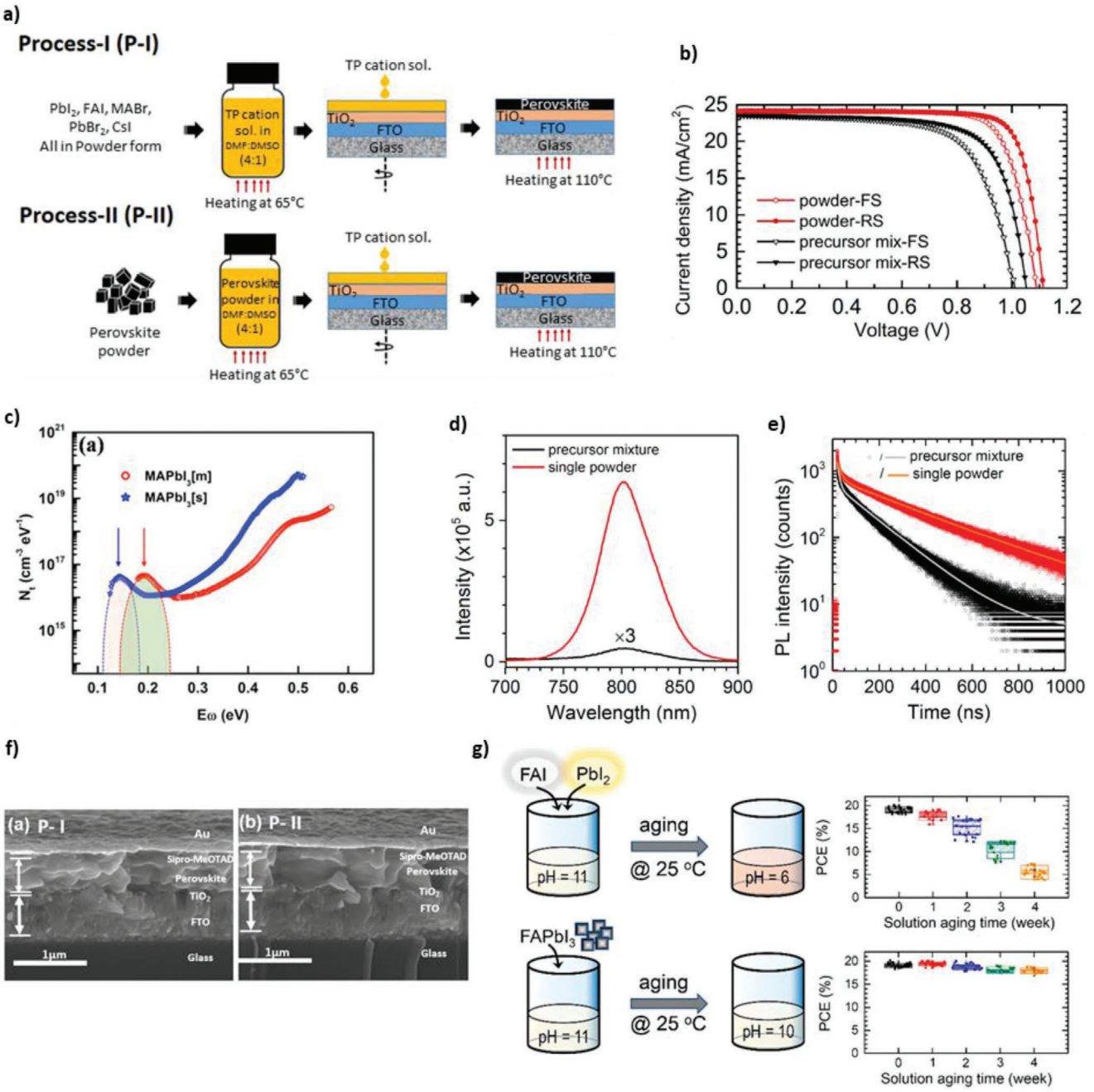

Figure 8. a) Schematic for preparing perovskite films with two different processes. P-I: perovskite film fabricated from the triple-cation perovskite precursor solution. P-II: perovskite film fabricated from the perovskite precursor solution prepared from perovskite powder. b) Solar cell IV curves of perovskite films prepared using synthesized single $FAPbI_3$ powder and the conventional precursor mixture (FAI + PbI_2). c) Defect densities distribution in $MAPbI_3$ based perovskite solar cells deduced from capacitance versus frequency at 300 K plotted versus energy where the $MAPbI_3$ films were processed on basis of dissolved mechanochemically synthesized powder-$MAPbI_3$(m) and on basis of MAI und PbI_2 precursors -$MAPbI_3$(s). The lower and higher energies correspond to shallow and deeper defect energy levels. d) Steady-state photoluminescence, and e) time-resolved photoluminescence (TRPL) for perovskite films prepared using synthesized single $FAPbI_3$ powder and the conventional precursor mixture (FAI + PbI_2), as well as corresponding solar cell IV curves (b). f) Cross-sectional FESEM images fabricated with P-I and P-II perovskite films as illustrated in (a). g) Illustration of solution aging experiments, where within 4 weeks, the pH value of conventional precursor mixtures of FAI and PbI_2 decreased from 11 to 6, while the pH value of stock solutions based on presynthesized $FAPbI_3$ stayed nearly unchanged within the same time period. a) Adapted and f) Reproduced with permission.[40] Copyright 2019, American Chemical Society. b,d,e) Reproduced with permission.[41] Copyright 2020, American Chemical Society. c) Reproduced with permission.[122] Copyright 2017, American Chemical Society. g) Reproduced with permission.[128] Copyright 2020, American Chemical Society.

sulfoxide (DMSO)/DMF mixture.[128] For solutions with individually solved precursors, the solution pH value changed from 11 to 6, i.e., from basic to slightly acidic within 4 weeks. This effect was significantly less pronounced (pH value change from 11 to 10 within 4 weeks) for a solution based on previously synthesized, and then dissolved δ-$FAPbI_3$ powder. Solar cells made from these solutions were stable, mainly independent of the aging of the redissolved-powder-solution (Figure 8g).[128]

4.2. Outlook Dissolved Perovskite Powders

The improved properties of perovskite layers and corresponding device performances when redissolved-powder-solutions (instead of the individual precursors) are used appears promising and is likely to attract more research interest. It also became clear that already the properties of dissolved-powder-solutions and precursor-based-solutions differ. Even though some papers have addressed this topic in the past, a general, cross-stoichiometric understanding of the exact powder-based solution properties has not yet developed. Here it will be important to develop a more detailed understanding of the solution chemistry of perovskite solutions. In addition, we note that little has been reported to date regarding the solubility of perovskite powder. In the respective papers it rather appears that dissolving perovskite powders is as easy as dissolving the precursor powders. In our experience, however, dissolving mixed perovskite powders in particular can be difficult, and further steps such as heating, stirring or filtering are necessary to achieve full dissolution. It is not yet clear which exact role the properties of the perovskite powders (e.g., particle size) or of the precursor materials (e.g., purity), or the powder synthesis route plays. In this context, the work of Choi et al. represents an interesting starting point.[130] For the synthesis of perovskite powder via precipitation they show that depending on the anti-solvent used, the perovskite powders exhibits different structural properties that strongly affect the morphology and structure of resulting $MAPbI_3$ thin films and, hence, the performance of the photovoltaic devices based on them.[130]

4.3. Suspension Deposition

Here, we are referring to the processing of dispersed perovskite powder in a liquid, which can be achieved by adding the powder to a nonsolvent or an antisolvent such as cyclohexane. In the past, such suspensions were mostly used to produce test layers or test devices, so that the processing of powder suspensions was not in the focus at first. For instance, Lopez et al. simply drop cast a suspension of mechanochemically synthesized $CsPbBr_3$ powder in DMSO onto an electrode-structured substrate, whereby photodetectors with high responsivity of 3 A W^{-1} at 420 nm could be demonstrated.[32] A slightly more sophisticated approach was used by Chen et al., who mixed different mechanochemically produced methylammonium lead halide perovskite powders in cyclohexane and toluene together with polymethyl methacrylate (PMMA) (powder/PMMA weight ratio 1/10) and deposited homogeneous layers via drop-casting. Using this approach, it was also possible to process different layers on top of each other, where the involved layers contained perovskites with different stoichiometry, so that high quality UV-pumped white light could be achieved (**Figure 9**a).[131]

Following a similar motivation, Xie et al. recently used two different ball milled cesium copper halide perovskite powders and mixed them with thermally curable silicone resin. Adding hardener resulted in a powder paste that could then be deposited on a UV-LED chip leading to a dual emission LED device.[134]

The processing of layers with the help of perovskite powder suspensions was also investigated in more detail in the past. Peng et al. used perovskite powder made from crushed $MAPbI_3$ single crystals and mixed it in PMMA, but with a significantly higher proportion of powder (powder/PMMA weight ratio 200/10) compared to Chen et al (powder/PMMA weight ratio 1/10[131]).[135] By spin coating, 11 µm thick layers of the perovskite/PMMA composite could be produced with a relatively low surface roughness of 78 nm. Using these layers, efficient thick junction photodiodes with fast light response of 800 ns could be demonstrated. Notably, the powder-based composite film was significantly more stable than a reference layer produced by solution processing without PMMA, both with respect to light-induced PL degradation of the neat layers and with respect to the temporal stability of photo- and dark current in the detector device.[135] Using the same processing approach, Peng et al. produced 14 µm thick $MAPbBr_3$/PMMA composite films in a recently published follow-up work (Figure 9b).[132] The resulting X-ray detectors showed reasonable device metrics (lowest detectable X-ray dose rate of 2.3 $\mu Gy_{air}\ s^{-1}$ and X-ray sensitivity of 488 $\mu C\ Gy_{air}^{-1}\ cm^{-2}$ under a low bias of -0.5 V). Also in this case, a high device stability with only small changes of the photocurrent after 50 d was observed.[132] In the field of perovskite-based X-ray detectors, using perovskites as scintillator material has gained enormous momentum over the past two years.[136–138] Gandini et al. recently manufactured reabsorption-free waveguiding plastic scintillators based on PMMA composites with $CsPbBr_3$ nanocrystal powders as scintillator and a perylene dyad as emitter material.[139] Here, the scintillation process turned out to be very efficient, with perylene dyad PL decay times of only a few ns in the red wavelength range (PL peak ≈ 600 nm). This was achieved due to the efficient blending of the $CsPbBr_3$ nanocrystal powders into PMMA that did not lead to any noticeable deterioration of the perovskite PL while ensuring a complete energy transfer to the perylene.[139]

In addition to introducing perovskite powders into a host matrix, other approaches for wet perovskite powder film processing have been demonstrated in the past as well. In 2016, Nejand et al. used $MAPbI_3$ powder homogenized by ball milling and successfully sprayed it onto different transport layers in a wet spraying process involving isopropanol.[133] These wet-sprayed layers were hot-pressed in a subsequent processing step with the help of a Teflon stamp, which further compacted the perovskite layer (Figure 9c). After optimizing the spraying and pressing process, solar cell efficiencies of up to 9% were achieved in a FTO/TiO_2/$MAPbI_3$/Spiro-MeOTAD/Au architecture.[133] Similarly, by wet processing $MAPbI_3$ powder and subsequent hot pressing using a Teflon stamp, Pitchaiya

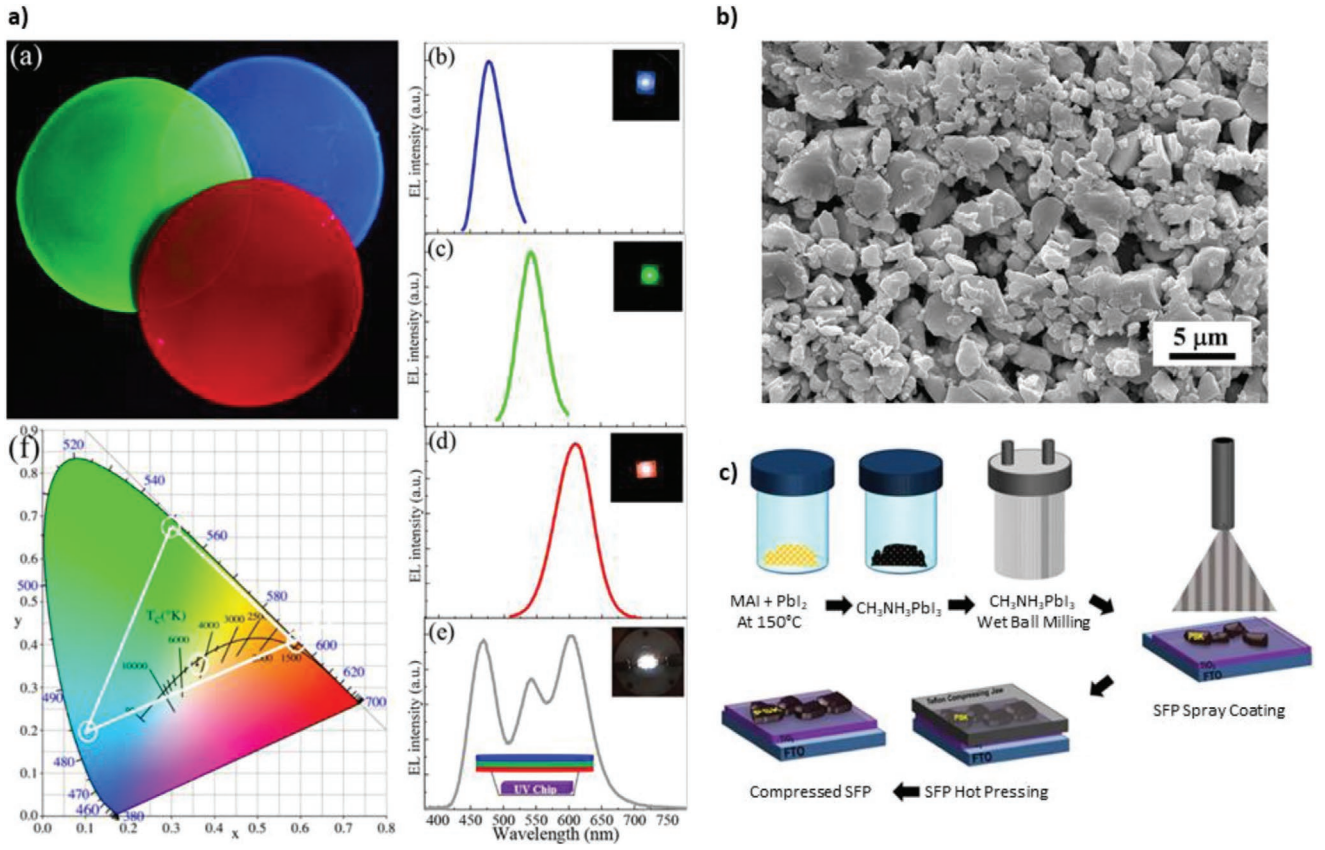

Figure 9. a) Luminescence photographs of blue-emitting, green-emitting, and red-emitting $MAPbX_3$ powders dispersed in PMMA films. EL spectra of LED devices constructed by coupling blue, green, and red perovskite/PMMA composite films and their combination with UV chip as well as CIE chromaticity coordinates of the LED devices in operation. b) Typical SEM image of $MAPbBr_3$ crystal/PMMA composite films. c) Schematic of the synthesizing and the deposition process of perovskite thin films using a wet spraying and subsequent pressing approach. a) Reproduced with permission.[131] Copyright 2019, American Chemical Society. b) Reproduced with permission.[132] Copyright 2020, Elsevier B.V. c) Adapted under the terms of the CC-BY 4.0 license.[133] Copyright 2016, the authors. Published by Nature Publications.

et al. achieved solar cells with 3.9% efficiency, but here the powder suspension was distributed on the substrate not by wet spraying but more simply by drop-casting.[140]

4.4. Outlook Direct Wet Powder Processing

Regarding powder suspension processing involving additional PMMA, it would be interesting to explore in the future to what extent this processing method allows to produce compact layers with reduced layer thicknesses, so that such layers could be used in thin film devices like LEDs or solar cells. From the previous works that followed the wet distribution of perovskite powder with subsequent pressure treatment, it already could be seen that this powder-based processing approach work, even though both processes, i.e., the deposition of the powder particles, as well as the pressing process, exhibit potential to be investigated, understood, and further optimized more in the future. In this context, it is worth noting that the pressure levels of <1 MPa as they were used for the pressing steps in the past, are significantly lower than the pressures in the range of 10 MPa, which have been used recently to successfully improve the morphology, compactness and optoelectronic properties of perovskite thin films.[108–111]

5. Summary and Outlook

In this progress report, we highlighted the latest developments in the field of halide perovskites in powder form and their powder-based processing. Both wet as well as dry powder processing approaches show high potential to fabricate high quality perovskite layers. However, the various approaches also clearly have existing limitations, e.g., regarding achievable layer thicknesses, compactness, and particle sizes, but also regarding the transferability of the powder properties into the film. To overcome the individual limitations, combining powder-based processing approaches with further posttreatments, e.g., by hot pressing, could be an important step in the future. For example, it would be highly attractive to be able to manufacture high-quality perovskite thin films completely dry on the basis of perovskite powder, which could then be used in efficient optoelectronic thin-film devices such as solar cells or LEDs. In combination with a better understanding of perovskite powder

passivation, powder processing methods such as powder aerosol deposition could also play a role to realize novel hetero layer structures, as they would be a desirable goal to realize energy resolved X-ray detectors.[8] In view of the rapid developments within the past few years, it will be exciting to see which further potentials powder-based halide perovskite processing will show in the future and how these powder-based methods can establish as real alternative to the conventional halide perovskite processing methods.

Acknowledgements

The authors acknowledge financial support by the German National Science Foundation DFG via the project PA 3373/3-1 and MO 1060/32-1. The authors further thank Prof. Ralf Moos, Prof. Anna Köhler, Dr. Paul Pistor and Konstantin Schötz for proof reading.

Open access funding enabled and organized by Projekt DEAL.

Conflict of Interest

The authors declare no conflict of interest.

Keywords

aerosol deposition, evaporation, hot pressing, melt processing, solvent free

Received: August 28, 2020
Revised: December 23, 2020
Published online: January 15, 2021

[1] H.-S. Kim, C.-R. Lee, J.-H. Im, K.-B. Lee, T. Moehl, A. Marchioro, S.-J. Moon, R. Humphry-Baker, J.-H. Yum, J. E. Moser, M. Grätzel, N.-G. Park, *Sci. Rep.* **2012**, *2*, 591.
[2] M. M. Lee, J. Teuscher, T. Miyasaka, T. N. Murakami, H. J. Snaith, *Science* **2012**, *338*, 643.
[3] National Renewable Energy Laboratory (NREL), Best Research-Cell Efficiency Chart, https://www.nrel.gov/pv/assets/pdfs/best-research-cell-efficiencies.20200925.pdf, (accessed: December 2020).
[4] K. Lin, J. Xing, L. N. Quan, F. P. G. de Arquer, X. Gong, J. Lu, L. Xie, W. Zhao, D. Zhang, C. Yan, W. Li, X. Liu, Y. Lu, J. Kirman, E. H. Sargent, Q. Xiong, Z. Wei, *Nature* **2018**, *562*, 245.
[5] W. Xu, Q. Hu, S. Bai, C. Bao, Y. Miao, Z. Yuan, T. Borzda, A. J. Barker, E. Tyukalova, Z. Hu, M. Kawecki, H. Wang, Z. Yan, X. Liu, X. Shi, K. Uvdal, M. Fahlman, W. Zhang, M. Duchamp, J.-M. Liu, A. Petrozza, J. Wang, L.-M. Liu, W. Huang, F. Gao, *Nat. Photonics* **2019**, *13*, 418.
[6] L. Gao, Q. Yan, *Sol. RRL* **2020**, *4*, 1900210.
[7] H. Wei, J. Huang, *Nat. Commun.* **2019**, *10*, 1066.
[8] M. Sytnyk, S. Deumel, S. F. Tedde, G. J. Matt, W. Heiss, *Appl. Phys. Lett.* **2019**, *115*, 190501.
[9] A. K. Jena, A. Kulkarni, T. Miyasaka, *Chem. Rev.* **2019**, *119*, 3036.
[10] L. Qiu, S. He, L. K. Ono, S. Liu, Y. Qi, *ACS Energy Lett.* **2019**, *4*, 2147.
[11] National Renewable Energy Laboratory (NREL), Champion Photovoltaic Module Efficiency Chart, https://www.nrel.gov/pv/assets/pdfs/champion-module-efficiencies.20200708.pdf (accessed: December 2020).
[12] C. B. Carter, M. G. Norton, in *Ceramic Materials: Powders, Fibers, Platelets, and Composites*, Springer, New York **2013**, https://doi.org/10.1007/978-1-4614-3523-5_20.
[13] C. B. Carter, M. G. Norton, in *Ceramic Materials: Coatings and Thick Films*, Springer, New York **2013**, https://doi.org/10.1007/978-1-4614-3523-5_27.
[14] D. Prochowicz, M. Saski, P. Yadav, M. Grätzel, J. Lewiński, *Acc. Chem. Res.* **2019**, *52*, 3233.
[15] F. Palazon, Y. El Ajjouri, H. J. Bolink, *Adv. Energy Mater.* **2020**, *10*, 1902499.
[16] Z. Hong, D. Tan, R. A. John, Y. K. E. Tay, Y. K. T. Ho, X. Zhao, T. C. Sum, N. Mathews, F. García, H. S. Soo, *iScience* **2019**, *16*, 312.
[17] P. Pal, S. Saha, A. Banik, A. Sarkar, K. Biswas, *Chem. – Eur. J.* **2018**, *24*, 1811.
[18] D. Prochowicz, P. Yadav, M. Saliba, M. Saski, S. M. Zakeeruddin, J. Lewiński, M. Grätzel, *Sustainable Energy Fuels* **2017**, *1*, 689.
[19] A. D. Jodlowski, A. Yépez, R. Luque, L. Camacho, G. de Miguel, *Angew. Chem., Int. Ed.* **2016**, *55*, 14972.
[20] N. Leupold, K. Schötz, S. Cacovich, I. Bauer, M. Schultz, M. Daubinger, L. Kaiser, A. Rebai, J. Rousset, A. Köhler, P. Schulz, R. Moos, F. Panzer, *ACS Appl. Mater. Interfaces* **2019**, *11*, 30259.
[21] C. C. Stoumpos, C. D. Malliakas, M. G. Kanatzidis, *Inorg. Chem.* **2013**, *52*, 9019.
[22] S. Tang, X. Xiao, J. Hu, B. Gao, H. Chen, Z. Peng, J. Wen, M. Era, D. Zou, *ChemPlusChem* **2020**, *85*, 240.
[23] A. M. Askar, A. Karmakar, G. M. Bernard, M. Ha, V. V. Terskikh, B. D. Wiltshire, S. Patel, J. Fleet, K. Shankar, V. K. Michaelis, *J. Phys. Chem. Lett.* **2018**, *9*, 2671.
[24] D. J. Kubicki, D. Prochowicz, A. Hofstetter, P. Péchy, S. M. Zakeeruddin, M. Grätzel, L. Emsley, *J. Am. Chem. Soc.* **2017**, *139*, 10055.
[25] A. Jana, M. Mittal, A. Singla, S. Sapra, *Chem. Commun.* **2017**, *53*, 3046.
[26] D. J. Kubicki, D. Prochowicz, A. Hofstetter, M. Saski, P. Yadav, D. Bi, N. Pellet, J. Lewiński, S. M. Zakeeruddin, M. Grätzel, L. Emsley, *J. Am. Chem. Soc.* **2018**, *140*, 3345.
[27] M. Wilke, N. Casati, *Chem. - Eur. J.* **2018**, *24*, 17701.
[28] D. J. Kubicki, D. Prochowicz, A. Hofstetter, S. M. Zakeeruddin, M. Grätzel, L. Emsley, *J. Am. Chem. Soc.* **2017**, *139*, 14173.
[29] B. Dou, L. M. Wheeler, J. A. Christians, D. T. Moore, S. P. Harvey, J. J. Berry, F. S. Barnes, S. E. Shaheen, M. F. A. M. van Hest, *ACS Energy Lett.* **2018**, *3*, 979.
[30] A. Boziki, D. J. Kubicki, A. Mishra, S. Meloni, L. Emsley, M. Grätzel, U. Rothlisberger, *Chem. Mater.* **2020**, *32*, 2605.
[31] F. Palazon, Y. E.l Ajjouri, P. Sebastia-Luna, S. Lauciello, L. Manna, H. J. Bolink, *J. Mater. Chem. C* **2019**, *7*, 11406.
[32] C. A. López, C. Abia, M. C. Alvarez-Galván, B.-K. Hong, M. V. Martínez-Huerta, F. Serrano-Sánchez, F. Carrascoso, A. Castellanos-Gómez, M. T. Fernández-Díaz, J. A. Alonso, *ACS Omega* **2020**, *5*, 5931.
[33] A. Karmakar, M. S. Dodd, X. Zhang, M. S. Oakley, M. Klobukowski, V. K. Michaelis, *Chem. Commun.* **2019**, *55*, 5079.
[34] L. Protesescu, S. Yakunin, O. Nazarenko, D. N. Dirin, M. V. Kovalenko, *ACS Appl. Nano Mater.* **2018**, *1*, 1300.
[35] M. Saski, D. Prochowicz, W. Marynowski, J. Lewiński, *Eur. J. Inorg. Chem.* **2019**, *2019*, 2680.
[36] Y. E.l Ajjouri, F. Locardi, M. C. Gélvez-Rueda, M. Prato, M. Sessolo, M. Ferretti, F. C. Grozema, F. Palazon, H. J. Bolink, *Energy Technol.* **2020**, *8*, 1900788.
[37] P. Sebastia-Luna, J. Navarro-Alapont, M. Sessolo, F. Palazon, H. J. Bolink, *Chem. Mater.* **2019**, *31*, 10205.
[38] Y. E.l Ajjouri, V. S. Chirvony, N. Vassilyeva, M. Sessolo, F. Palazon, H. J. Bolink, *J. Mater. Chem. C* **2019**, *7*, 6236.
[39] D. Prochowicz, P. Yadav, M. Saliba, D. J. Kubicki, M. M. Tavakoli, S. M. Zakeeruddin, J. Lewiński, L. Emsley, M. Grätzel, *Nano Energy* **2018**, *49*, 523.
[40] R. Singh, S. Sandhu, H. Yadav, J.-J. Lee, *ACS Appl. Mater. Interfaces* **2019**, *11*, 29941.

[41] Y. Zhang, S. Seo, S. Y. Lim, Y. Kim, S.-G. Kim, D.-K. Lee, S.-H. Lee, H. Shin, H. Cheong, N.-G. Park, *ACS Energy Lett.* **2020**, *5*, 360.
[42] L.-C. Chen, Z.-L. Tseng, S.-Y. Chen, S. Yang, *Ceram. Int.* **2017**, *43*, 16032.
[43] Y. Liu, S. Akin, A. Hinderhofer, F. T. Eickemeyer, H. Zhu, J. Y. Seo, J. Zhang, F. Schreiber, H. Zhang, S. M. Zakeeruddin, A. Hagfeldt, M. I. Dar, M. Grätzel, *Angew. Chem., Int. Ed.* **2020**, *59*, 15688.
[44] T. P. Gujar, T. Unger, A. Schönleber, M. Fried, F. Panzer, S. van Smaalen, A. Köhler, M. Thelakkat, *Phys. Chem. Chem. Phys.* **2018**, *20*, 605.
[45] C. A. López, M. C. Alvarez-Galván, M. V. Martínez-Huerta, F. Fauth, J. A. Alonso, *CrystEngComm* **2020**, *22*, 767.
[46] J.-W. Lee, S.-G. Kim, S.-H. Bae, D.-K. Lee, O. Lin, Y. Yang, N.-G. Park, *Nano Lett.* **2017**, *17*, 4270.
[47] Y. Shao, Y. Fang, T. Li, Q. Wang, Q. Dong, Y. Deng, Y. Yuan, H. Wei, M. Wang, A. Gruverman, J. Shield, J. Huang, *Energy Environ. Sci.* **2016**, *9*, 1752.
[48] P. Zhao, B. J. Kim, H. S. Jung, *Mater. Today Energy* **2018**, *7*, 267.
[49] M. M. Tavakoli, W. Tress, J. V. Milić, D. Kubicki, L. Emsley, M. Grätzel, *Energy Environ. Sci.* **2018**, *11*, 3310.
[50] L. Martínez-Sarti, F. Palazon, M. Sessolo, H. J. Bolink, *Adv. Opt. Mater.* **2020**, *8*, 1901494.
[51] B. A. Rosales, L. Wei, J. Vela, *J. Solid State Chem.* **2019**, *271*, 206.
[52] H. Xie, S. Hao, J. Bao, T. J. Slade, G. J. Snyder, C. Wolverton, M. G. Kanatzidis, *J. Am. Chem. Soc.* **2020**, *142*, 9553.
[53] Y. Liu, Z. Yang, D. Cui, X. Ren, J. Sun, X. Liu, J. Zhang, Q. Wei, H. Fan, F. Yu, X. Zhang, C. Zhao, S. Liu, *Adv. Mater.* **2015**, *27*, 5176.
[54] W. Pan, B. Yang, G. Niu, K.-H. Xue, X. Du, L. Yin, M. Zhang, H. Wu, X.-S. Miao, J. Tang, *Adv. Mater.* **2019**, *31*, 1904405.
[55] B. A. Rosales, L. Men, S. D. Cady, M. P. Hanrahan, A. J. Rossini, J. Vela, *Chem. Mater.* **2016**, *28*, 6848.
[56] S. Shrestha, R. Fischer, G. J. Matt, P. Feldner, T. Michel, A. Osvet, I. Levchuk, B. Merle, S. Golkar, H. Chen, S. F. Tedde, O. Schmidt, R. Hock, M. Rührig, M. Göken, W. Heiss, G. Anton, C. J. Brabec, *Nat. Photonics* **2017**, *11*, 436.
[57] F. Zhu, L. Men, Y. Guo, Q. Zhu, U. Bhattacharjee, P. M. Goodwin, J. W. Petrich, E. A. Smith, J. Vela, *ACS Nano* **2015**, *9*, 2948.
[58] M. C. Alvarez-Galván, J. A. Alonso, C. A. López, E. López-Linares, C. Contreras, M. J. Lázaro, F. Fauth, M. V. Martínez-Huerta, *Cryst. Growth Des.* **2019**, *19*, 918.
[59] X. Jia, Z. Hu, Y. Zhu, T. Weng, J. Wang, J. Zhang, Y. Zhu, *J. Alloys Compd.* **2017**, *725*, 270.
[60] V. Bhooshan Kumar, L. Gouda, Z. e. Porat, A. Gedanken, *Ultrason. Sonochem.* **2016**, *32*, 54.
[61] D. M. Jang, D. H. Kim, K. Park, J. Park, J. W. Lee, J. K. Song, *J. Mater. Chem. C* **2016**, *4*, 10625.
[62] H. Jiang, C. Wang, C. Lv, S. Xu, L. Zhu, R. Zhang, Y. Cui, *Mater. Res. Express* **2017**, *4*, 025038.
[63] Y. Tong, E. Bladt, M. F. Aygüler, A. Manzi, K. Z. Milowska, V. A. Hintermayr, P. Docampo, S. Bals, A. S. Urban, L. Polavarapu, J. Feldmann, *Angew. Chem., Int. Ed.* **2016**, *55*, 13887.
[64] K. V. Manukyan, A. V. Yeghishyan, D. O. Moskovskikh, J. Kapaldo, A. Mintairov, A. S. Mukasyan, *J. Mater. Sci.* **2016**, *51*, 9123.
[65] E. Aleksanyan, A. Aprahamian, A. S. Mukasyan, V. Harutyunyan, K. V. Manukyan, *J. Mater. Sci.* **2020**, *55*, 8665.
[66] D. Pérez-del-Rey, P. P. Boix, M. Sessolo, A. Hadipour, H. J. Bolink, *J. Phys. Chem. Lett.* **2018**, *9*, 1041.
[67] J. Ávila, C. Momblona, P. P. Boix, M. Sessolo, H. J. Bolink, *Joule* **2017**, *1*, 431.
[68] P.-S. Shen, Y.-H. Chiang, M.-H. Li, T.-F. Guo, P. Chen, *APL Mater.* **2016**, *4*, 091509.
[69] M. Sessolo, C. Momblona, L. Gil-Escrig, H. J. Bolink, *MRS Bull.* **2015**, *40*, 660.
[70] M. J. Bækbo, O. Hansen, I. Chorkendorff, P. C. K. Vesborg, *RSC Adv.* **2018**, *8*, 29899.
[71] P. Fan, D. Gu, G.-X. Liang, J.-T. Luo, J.-L. Chen, Z.-H. Zheng, D.-P. Zhang, *Sci. Rep.* **2016**, *6*, 29910.
[72] Y. E.l Ajjouri, F. Palazon, M. Sessolo, H. J. Bolink, *Chem. Mater.* **2018**, *30*, 7423.
[73] M. J. Crane, D. M. Kroupa, J. Y. Roh, R. T. Anderson, M. D. Smith, D. R. Gamelin, *ACS Appl. Energy Mater.* **2019**, *2*, 4560.
[74] Y. El Ajjouri, A. M. Igual-Muñoz, M. Sessolo, F. Palazon, H. J. Bolink, *Adv. Opt. Mater.* **2020**, *8*, 2000423.
[75] V. M. Kiyek, Y. A. Birkhölzer, Y. Smirnov, M. Ledinsky, Z. Remes, J. Momand, B. J. Kooi, G. Koster, G. Rijnders, M. Morales-Masis, *Adv. Mater. Interfaces* **2020**, *7*, 2000162.
[76] C. Borri, N. Calisi, E. Galvanetto, N. Falsini, F. Biccari, A. Vinattieri, G. Cucinotta, S. Caporali, *Nanomaterials* **2020**, *10*, 60.
[77] D. B. Mitzi, D. R. Medeiros, P. W. DeHaven, *Chem. Mater.* **2002**, *14*, 2839.
[78] D. B. Mitzi, C. D. Dimitrakopoulos, J. Rosner, D. R. Medeiros, Z. Xu, C. Noyan, *Adv. Mater.* **2002**, *14*, 1772.
[79] T. Li, W. A. Dunlap-Shohl, Q. Han, D. B. Mitzi, *Chem. Mater.* **2017**, *29*, 6200.
[80] T. Li, W. A. Dunlap-Shohl, E. W. Reinheimer, P. L.e Magueres, D. B. Mitzi, *Chem. Sci.* **2019**, *10*, 1168.
[81] T. Li, A. M. Zeidell, G. Findik, W. A. Dunlap-Shohl, J. Euvrard, K. Gundogdu, O. D. Jurchescu, D. B. Mitzi, *Chem. Mater.* **2019**, *31*, 4267.
[82] Y. He, L. Matei, H. J. Jung, K. M. McCall, M. Chen, C. C. Stoumpos, Z. Liu, J. A. Peters, D. Y. Chung, B. W. Wessels, M. R. Wasielewski, V. P. Dravid, A. Burger, M. G. Kanatzidis, *Nat. Commun.* **2018**, *9*, 1609.
[83] G. J. Matt, I. Levchuk, J. Knüttel, J. Dallmann, A. Osvet, M. Sytnyk, X. Tang, J. Elia, R. Hock, W. Heiss, C. J. Brabec, *Adv. Mater. Interfaces* **2020**, *7*, 1901575.
[84] C. C. Stoumpos, C. D. Malliakas, J. A. Peters, Z. Liu, M. Sebastian, J. Im, T. C. Chasapis, A. C. Wibowo, D. Y. Chung, A. J. Freeman, B. W. Wessels, M. G. Kanatzidis, *Cryst. Growth Des.* **2013**, *13*, 2722.
[85] J. Song, Q. Cui, J. Li, J. Xu, Y. Wang, L. Xu, J. Xue, Y. Dong, T. Tian, H. Sun, H. Zeng, *Adv. Opt. Mater.* **2017**, *5*, 1700157.
[86] P. Zhang, Q. Sun, Y. Xu, X. Li, L. Liu, G. Zhang, X. Tao, *Cryst. Growth Des.* **2020**, *20*, 2424.
[87] K. Schötz, A. M. Askar, W. Peng, D. Seeberger, T. P. Gujar, M. Thelakkat, A. Köhler, S. Huettner, O. M. Bakr, K. Shankar, F. Panzer, *J. Mater. Chem. C* **2020**, *8*, 2289.
[88] K. Schötz, A. M. Askar, A. Köhler, K. Shankar, F. Panzer, *Adv. Opt. Mater.* **2020**, *8*, 2000455.
[89] P. Fassl, V. Lami, F. J. Berger, L. M. Falk, J. Zaumseil, B. S. Richards, I. A. Howard, Y. Vaynzof, U. W. Paetzold, arXiv:2010.12950 [physics. app-ph] **2020**.
[90] F. Deschler, M. Price, S. Pathak, L. E. Klintberg, D.-D. Jarausch, R. Higler, S. Hüttner, T. Leijtens, S. D. Stranks, H. J. Snaith, M. Atatüre, R. T. Phillips, R. H. Friend, *J. Phys. Chem. Lett.* **2014**, *5*, 1421.
[91] M. Yang, Y. Zeng, Z. Li, D. H. Kim, C.-S. Jiang, J. van de Lagemaat, K. Zhu, *Phys. Chem. Chem. Phys.* **2017**, *19*, 5043.
[92] T. Kirchartz, J. A. Márquez, M. Stolterfoht, T. Unold, *Adv. Energy Mater.* **2020**, *10*, 1904134.
[93] S. H. Cho, Y. J. Yoon, *Thin Solid Films* **2013**, *547*, 91.
[94] J.-J. Park, J.-G. Lee, S. C. James, S. S. Al-Deyab, S. Ahn, S. S. Yoon, *Comput. Mater. Sci.* **2015**, *101*, 66.

[95] J.-J. Park, J.-G. Lee, D.-Y. Kim, J.-H. Lee, J. H. Yun, J. Gwak, Y.-J. Eo, A. Cho, M. T. Swihart, S. S. Al-Deyab, S. Ahn, D. Kim, S. S. Yoon, *Acta Mater.* **2017**, *123*, 44.
[96] Y. Imanaka, J. Akedo, *Int. J. Appl. Ceram. Technol.* **2010**, *7*, E23.
[97] M. Bektas, T. Stöcker, A. Mergner, G. Hagen, R. Moos, *J. Sens. Sens. Syst.* **2018**, *7*, 289.
[98] H. Kim, S. Yang, S.-H. Ahn, C. S. Lee, *Thin Solid Films* **2016**, *600*, 109.
[99] M. Shimizu, H. Usui, H. Sakaguchi, *J. Power Sources* **2014**, *248*, 378.
[100] J. Exner, M. Schubert, D. Hanft, J. Kita, R. Moos, *J. Eur. Ceram. Soc.* **2019**, *39*, 592.
[101] J. Akedo, *J. Therm. Spray Technol.* **2008**, *17*, 181.
[102] D. Hanft, J. Exner, M. Schubert, T. Stöcker, P. Fuierer, R. Moos, *J. Ceram. Sci. Technol.* **2015**, *6*, 147.
[103] M. Schubert, D. Hanft, T. Nazarenus, J. Exner, M. Schubert, P. Nieke, P. Glosse, N. Leupold, J. Kita, R. Moos, *Funct. Mater. Lett.* **2019**, *12*, 1930005.
[104] J. Akedo, *J. Ceram. Soc. Jpn.* **2020**, *128*, 101.
[105] F. Panzer, D. Hanft, T. Gujar, F.-J. Kahle, M. Thelakkat, A. Köhler, R. Moos, *Materials* **2016**, *9*, 277.
[106] S. Kim, M.-Y. Cho, I.-S. Kim, W.-J. Kim, S.-H. Park, S. Baek, J.-M. Oh, S.-W. Kim, *Adv. Mater. Interfaces* **2019**, *6*, 1900359.
[107] M.-Y. Cho, S. Kim, I.-S. Kim, E.-S. Kim, Z.-J. Wang, N.-Y. Kim, S.-W. Kim, J.-M. Oh, *Adv. Funct. Mater.* **2020**, *30*, 1907449.
[108] N. Pourdavoud, T. Haeger, A. Mayer, P. J. Cegielski, A. L. Giesecke, R. Heiderhoff, S. Olthof, S. Zaefferer, I. Shutsko, A. Henkel, D. Becker-Koch, M. Stein, M. Cehovski, O. Charfi, H.-H. Johannes, D. Rogalla, M. C. Lemme, M. Koch, Y. Vaynzof, K. Meerholz, W. Kowalsky, H.-C. Scheer, P. Görrn, T. Riedl, *Adv. Mater.* **2019**, *31*, 1903717.
[109] B. Abdollahi Nejand, S. Gharibzadeh, V. Ahmadi, H. R. Shahverdi, *J. Phys. Chem. C* **2016**, *120*, 2520.
[110] J. Xiao, Y. Yang, X. Xu, J. Shi, L. Zhu, S. Lv, H. Wu, Y. Luo, D. Li, Q. Meng, *J. Mater. Chem. A* **2015**, *3*, 5289.
[111] N. Pourdavoud, A. Mayer, M. Buchmüller, K. Brinkmann, T. Häger, T. Hu, R. Heiderhoff, I. Shutsko, P. Görrn, Y. Chen, H.-C. Scheer, T. Riedl, *Adv. Mater. Technol.* **2018**, *3*, 1700253.
[112] S. Tie, W. Zhao, D. Xin, M. Zhang, J. Long, Q. Chen, X. Zheng, J. Zhu, W. H. Zhang, *Adv. Mater.* **2020**, *32*, 2001981.
[113] C. Witt, A. Schmid, N. Leupold, M. Schultz, J. Höcker, A. Baumann, R. Moos, F. Panzer, *ACS Appl. Electron. Mater.* **2020**, *2*, 2619.
[114] B. Yang, W. Pan, H. Wu, G. Niu, J.-H. Yuan, K.-H. Xue, L. Yin, X. Du, X.-S. Miao, X. Yang, Q. Xie, J. Tang, *Nat. Commun.* **2019**, *10*, 1989.
[115] M. Hu, S. Jia, Y. Liu, J. Cui, Y. Zhang, H. Su, S. Cao, L. Mo, D. Chu, G. Zhao, K. Zhao, Z. Yang, S. F. Liu, *ACS Appl. Mater. Interfaces* **2020**, *12*, 16592.
[116] M. Xia, J.-H. Yuan, G. Niu, X. Du, L. Yin, W. Pan, J. Luo, Z. Li, H. Zhao, K.-H. Xue, X. Miao, J. Tang, *Adv. Funct. Mater.* **2020**, *30*, 1910648.
[117] H. Wei, Y. Fang, P. Mulligan, W. Chuirazzi, H.-H. Fang, C. Wang, B. R. Ecker, Y. Gao, M. A. Loi, L. Cao, J. Huang, *Nat. Photonics* **2016**, *10*, 333.
[118] T.-Y. Yang, G. Gregori, N. Pellet, M. Grätzel, J. Maier, *Angew. Chem., Int. Ed.* **2015**, *54*, 7905.
[119] C. Li, S. Tscheuschner, F. Paulus, P. E. Hopkinson, J. Kießling, A. Köhler, Y. Vaynzof, S. Huettner, *Adv. Mater.* **2016**, *28*, 2446.
[120] A. D. Sheikh, V. Vhanalakar, A. Katware, K. Pawar, P. S. Patil, *Adv. Mater. Technol.* **2019**, *4*, 1900251.
[121] H.-J. Yen, P.-W. Liang, C.-C. Chueh, Z. Yang, A. K. Y. Jen, H.-L. Wang, *ACS Appl. Mater. Interfaces* **2016**, *8*, 14513.
[122] D. Prochowicz, P. Yadav, M. Saliba, M. Saski, S. M. Zakeeruddin, J. Lewiński, M. Grätzel, *ACS Appl. Mater. Interfaces* **2017**, *9*, 28418.
[123] J. Wang, F. Meng, R. Li, S. Chen, X. Huang, J. Xu, X. Lin, R. Chen, H. Wu, H.-L. Wang, *Sol. RRL* **2020**, *4*, 2000091.
[124] D. Prochowicz, M. Franckevičius, A. M. Cieślak, S. M. Zakeeruddin, M. Grätzel, J. Lewiński, *J. Mater. Chem. A* **2015**, *3*, 20772.
[125] E. H. Jung, N. J. Jeon, E. Y. Park, C. S. Moon, T. J. Shin, T.-Y. Yang, J. H. Noh, J. Seo, *Nature* **2019**, *567*, 511.
[126] H. Min, M. Kim, S.-U. Lee, H. Kim, G. Kim, K. Choi, J. H. Lee, S. I. Seok, *Science* **2019**, *366*, 749.
[127] N. J. Jeon, H. Na, E. H. Jung, T.-Y. Yang, Y. G. Lee, G. Kim, H.-W. Shin, S. Il Seok, J. Lee, J. Seo, *Nat. Energy* **2018**, *3*, 682.
[128] G. S. Shin, Y. Zhang, N.-G. Park, *ACS Appl. Mater. Interfaces* **2020**, *12*, 15167.
[129] Y. Zhang, S.-G. Kim, D.-K. Lee, N.-G. Park, *ChemSusChem* **2018**, *11*, 1813.
[130] Y. C. Choi, S. W. Lee, D.-H. Kim, *APL Mater.* **2017**, *5*, 026101.
[131] D. Chen, J. Li, X. Chen, J. Chen, J. Zhong, *ACS Appl. Mater. Interfaces* **2019**, *11*, 10059.
[132] J. Peng, K. Ye, Y. Xu, L. Cui, R. Li, H. Peng, Q. Lin, *Sens. Actuators A* **2020**, *312*, 112132.
[133] B. A. Nejand, S. Gharibzadeh, V. Ahmadi, H. R. Shahverdi, *Sci. Rep.* **2016**, *6*, 33649.
[134] L. Xie, B. Chen, F. Zhang, Z. Zhao, X. Wang, L. Shi, Y. Liu, L. Huang, R. Liu, B. Zou, Y. Wang, *Photonics Res.* **2020**, *8*, 768.
[135] J. Peng, L. Cui, R. Li, Y. Xu, L. Jiang, Y. Li, W. Li, X. Tian, Q. Lin, *J. Mater. Chem. C* **2019**, *7*, 1859.
[136] Q. Chen, J. Wu, X. Ou, B. Huang, J. Almutlaq, A. A. Zhumekenov, X. Guan, S. Han, L. Liang, Z. Yi, J. Li, X. Xie, Y. Wang, Y. Li, D. Fan, D. B. L. Teh, A. H. All, O. F. Mohammed, O. M. Bakr, T. Wu, M. Bettinelli, H. Yang, W. Huang, X. Liu, *Nature* **2018**, *561*, 88.
[137] F. Cao, D. Yu, W. Ma, X. Xu, B. Cai, Y. M. Yang, S. Liu, L. He, Y. Ke, S. Lan, K.-L. Choy, H. Zeng, *ACS Nano* **2020**, *14*, 5183.
[138] V. B. Mykhaylyk, H. Kraus, M. Saliba, *Mater. Horiz.* **2019**, *6*, 1740.
[139] M. Gandini, I. Villa, M. Beretta, C. Gotti, M. Imran, F. Carulli, E. Fantuzzi, M. Sassi, M. Zaffalon, C. Brofferio, L. Manna, L. Beverina, A. Vedda, M. Fasoli, L. Gironi, S. Brovelli, *Nat. Nanotechnol.* **2020**, *15*, 462.
[140] S. Pitchaiya, M. Natarajan, A. Santhanam, V. Asokan, V. Madurai Ramakrishnan, Y. Selvaraj, A. Yuvapragasam, B. Rangasamy, S. Sundaram, D. Velauthapillai, *Mater. Res. Bull.* **2018**, *108*, 61.

Nico Leupold received his Master of Science in Materials Science and Engineering from the University of Bayreuth, Germany, in 2017. He is currently a Ph.D. student under the supervision of Dr. Fabian Panzer and Prof. Dr.-Ing. Ralf Moos at the Department of Functional Materials at the University of Bayreuth. His major research interest lies in the optimization of halide perovskite powders, the understanding of their optoelectronic properties and on film fabrication via the Powder Aerosol Deposition Method.

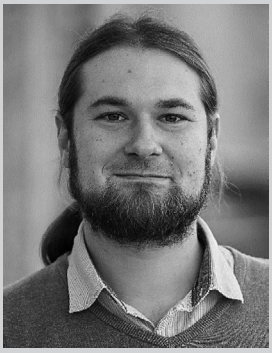

Fabian Panzer is Habilitation candidate and leads the perovskite subgroup within the Soft Matter Optoelectronics group at the University of Bayreuth. He completed his Diploma in Physics in 2013 at the University of Bayreuth, where he also obtained his Ph.D in 2016. His research focuses on understanding the processing of emerging semiconductors such as halide perovskites or organic semiconductors, for application in optoelectronic devices like solar cells or X-ray detectors.